EconomiX

The Unequal Burden of Heat: Spatial Heterogeneity in Productivity Responses in French Agriculture

Thomas Jacquet

2026-4 Document de Travail/ Working Paper

EconomiX - UMR 7235 Bâtiment Maurice Allais
Université Paris Nanterre 200, Avenue de la République
92001 Nanterre Cedex

Site Web : economix.fr
Contact : secreteriat@economix.fr

The Unequal Burden of Heat: Spatial Heterogeneity in Productivity Responses in French Agriculture

Thomas Jacquet[a,*]

[a]*University Paris Nanterre, EconomiX - CNRS*

Abstract

This article assesses the short- and medium-term effects of extreme heat on agricultural productivity across French departments during 1980-2023. Using high-resolution ERA5-Land temperature data and CORINE Land Cover, we construct a sector-specific Extreme Degree Days (EDD) index, weighted by cropland and pasture shares to capture sector-specific thermal stress. We estimate department-specific impulse responses via local projections and find significant and persistent productivity losses following heat shocks above 29 °C, with effects intensifying over a four-year horizon and attenuating only modestly thereafter. A Wald test confirms substantial regional heterogeneity in sensitivity to extreme temperatures. The negative impacts are particularly pronounced in lower-productivity, livestock-oriented departments clustered between 44.5° and 46° north latitude. These findings underscore the macroeconomic relevance of a spatially disaggregated measure of exposure to extreme temperatures and highlight the urgency of region-specific adaptation strategies as these episodes intensify.

Keywords: Agriculture; Climate change; Extreme heat; France; Productivity

JEL classification: O13; Q19; Q54

---

*Email adress: thomas.jacquet@parisnanterre.fr
We would like to thank Cécile Couharde and Rémi Generoso for their comments and advice as well as Ablam Estel Apeti, Souleymane Cissé, Michaël Guillossou, Chouaib Jouf, Adam Poupard and Albin Salmon for their valuable suggestions. Earlier versions of this paper were presented at the Parisian PhD Seminar on Economics and Environment (2024), the French Economic Association Annual Congress (2024), the International Symposium on Climate, Finance, and Sustainability (2024), the Annual Conference of the Natural Resources and Local Economy Chair (2025), and the Annual Conference of the European Association of Environmental and Resource Economists (2025). We thank participants and discussants for their thoughtful discussions and suggestions.

1 Introduction

France is undergoing a rapid climatic transformation (IPCC, 2021, 2022; Ribes et al., 2022). The past decade has been the warmest in the instrumental record, and the summers of 2023 and 2024 each set new national heatwave records (WMO, 2024, 2025). In response, the third National Adaptation Plan for Climate Change (PNACC-3) adopts a +4 °C warming trajectory for mainland France by 2100 as its reference scenario and emphasizes territorial disparities in vulnerability and adaptive capacity, calling for regionally tailored strategies (Ministère de la Transition écologique et de la Cohésion des territoires, 2025). For the food system, the High Council for Climate concludes that agriculture is already experiencing significant and intensifying climate impacts while still accounting for a substantial share of France's territorial and footprint emissions, and it argues that adaptation must avoid aggravating social and spatial inequalities and reflect the diversity of production systems and territories (Haut Conseil pour le Climat, 2024). Assessments for the European Parliament find large and spatially uneven agricultural losses from extreme events in the European Union and identify southern and south-western Europe, including large parts of France, as hotspots where heat and drought risks will intensify even under moderate warming paths (Devot et al., 2023). These diagnoses place heat stress in French agriculture firmly on the policy agenda and raise a central operational question: which departments and production systems are most exposed in terms of economic performance and over what horizons, so that adaptation support, water management and risk-sharing instruments can be targeted accordingly.

Despite the salience of this issue, there are, to our knowledge, no studies that quantify the dynamic effects of climatic extremes on agricultural performance outcomes across the national territory and their spatial heterogeneity at policy-relevant scales. An extensive empirical literature has quantified climate-yield relationships, showing that inter-annual weather variability and extreme events generate sizable yield losses and pronounced spatial patterns for major crops (van der Velde et al., 2012; Ceglar et al., 2016; Gammans et al., 2017; Zampieri et al., 2017; Ben-Ari et al., 2018; Schauberger et al., 2021; Nóia Júnior et al., 2023). This literature identify where and for which crops biophysical responses to heat and water stress are steepest and thereby provides essential evidence for agronomic decision-making and risk-management policy. However, it remains largely crop-specific and focused on yields rather than broader performance indicators. Moreover, it does not systematically relate production systems to spatial heterogeneity in economic outcomes, offering limited guidance on how extreme heat shocks translate into agricultural outcomes at territorially salient scales for public action.

In this article, we aim to advance the empirical literature on climate shocks in agriculture by providing the first estimates of the dynamic effects of extreme heat on agricultural labor productivity across the French territory and by explicitly characterizing the spatial heterogeneity of these responses. To make these estimates directly relevant for territorial policymaking, we focus on the French departmental level, which combines stable boundaries over time—facilitating the construction of consistent long-run climatic, agricultural and socio-economic series—with a central role in the territorial organization of public policy, notably in social assistance, transport, spatial planning and rural development. Climate shocks to agriculture at this level can thus simultaneously affect local production structures, labor markets and the fiscal capacity of the authorities responsible for delivering and co-financing adaptation and risk-management measures. Empirically, we study mainland France over 1980-2023, a period that spans major changes in climate, agricultural policy and farming systems. On the exposure side, we construct a sector-specific Extreme Degree Days (EDD) index that cumulates daily temperatures above agronomically relevant thresholds and weights grid-cell EDD by departmental cropland and pasture shares. This metric is grounded in evidence that crop yields decline sharply once daily temperatures exceed roughly 29-32 °C (Schlenker and Roberts, 2009; Lobell et al., 2011) and in a broader literature documenting adverse productivity effects of extreme heat in agriculture (D'Agostino and Schlenker, 2016). It therefore directly encodes nonlinear damages at high temperatures and spatial heterogeneity in production structures. On the econometric side, we implement a local projection framework with unit-specific coefficients at the departmental level to recover short- and medium-run impulse responses to thermal shocks. Local projections provide a flexible way to estimate dynamic responses without tightly specifying the underlying data-generating process, and recent work shows that relaxing slope homogeneity across units is crucial for uncovering the distribution of climate impacts rather than only their average (Berg et al., 2024).

Our results indicate that a one-unit increase in EDD above 29 °C lowers agricultural labor productivity contemporaneously and that effects remain negative in the short run and intensify at medium horizons, with only modest attenuation at the longest horizon. A Wald test strongly rejects slope homogeneity and confirms substantial regional heterogeneity in climate sensitivity. Spatially, the largest statistically significant and most persistent declines are concentrated in central and southern departments, in Corsica and in the western Grand Est, and we identify a critical inland band of elevated vulnerability between 44.5° and 46° north latitude that predominantly affects lower-productivity, livestock-oriented areas. These patterns are consistent with mechanisms emphasized in the climate and agronomy literature—physiological stress on crops and livestock, water stress via higher evapotranspiration and heat-related reductions in human labor capacity (Kjellstrom et al., 2016).

The article contributes to the literature and to current policy debates in two main ways. First, it uses a local projection framework tailored to estimate nonlinear temperature effects through sector-specific, land-use-weighted EDD measures that account for threshold-based heat stress and regional heterogeneity in economic structure, climate, agricultural specialization and adaptive capacity. Second, by applying this framework to French agriculture at the departmental scale, we move beyond crop-specific yield analyses and homogeneous response assumptions by providing evidence on labor productivity, a welfare-relevant outcome for territorial cohesion, farm incomes and the design of Common Agricultural Policy (CAP) and national adaptation instruments, with the aim of improving support for environmental and climate action (Midler and Pagnon, 2022). In doing so, we offer a policy-relevant characterization of French agricultural vulnerability to extreme heat, directly informing where structural adjustment and targeted adaptation support are most urgently needed.

The rest of the paper is organized as follows. Section 2 sets out the French departmental agro-climate context and conceptual framework. Section 3 describes the data and the construction of the sector-specific EDD index. Section 4 details the econometric strategy. Section 5 presents the main results, along with sensitivity analysis and robustness checks. Section 6 concludes with implications for regional climate adaptation, limitations of our results, and the design of agricultural and territorial policies.

2 Context and conceptual framework

2.1 French departmental agro-climate context

Departmental disparities in French agriculture are well documented. Several works show large gaps in value added per worker tied to land use, livestock intensity, capital and location, motivating analysis at the department scale and over time (Bonnieux and Rainelli, 1980; Bonnieux, 1982).

To characterize this production geography more precisely, we use the 2010 and 2020 Agricultural Census tables organized by the technical and economic organization of farms (OTEX) classification. It classifies farms by their main production orientation based on Standard Output (e.g. cereals/oleo-proteaginous, dairy, ruminants, horticulture, viticulture), so dominance reflects the activity generating the largest share of value. For each department, we compute the share of farms in each OTEX and identify the dominant orientation as the one with the largest share. Figure 1 shows the resulting map of main OTEX in 2010 and 2020 and highlights a stable but heterogeneous pattern—cereals and other field crops in the Paris Basin and parts of the southwest, ruminant systems in the Armorican and Central Massifs and the eastern departments, vineyards in the South, the Champagne and Bordeaux regions and a gradual shift toward more specialized systems in a subset of departments.

Figure 1: Main technical and economic organization of farms (OTEX) in 2010 and 2020

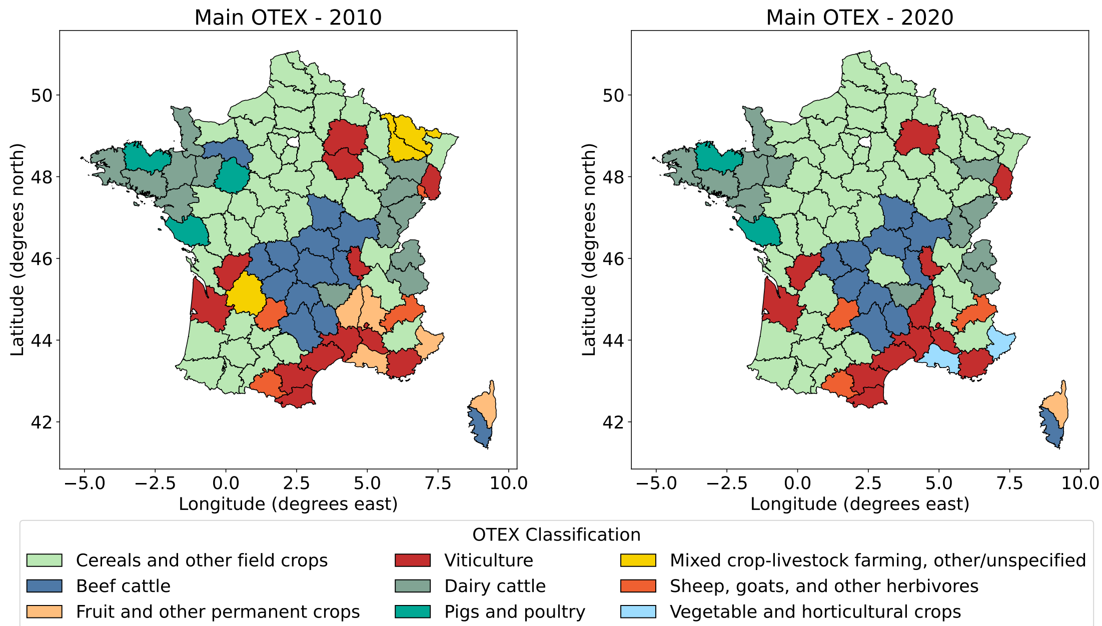

Note: We calculate the share of each category of technical and economic organization of farms for each department based on the number of farms in each category. The main OTEX is highlighted for 2010 (left) and 2020 (right). *Sources:* Agricultural Census 2010 and 2020.

In the northwest, oceanic regions such as Brittany and Normandy combine mild temperatures and ample rainfall with forage-based dairy and beef systems. The more semi-continental departments of the Paris Basin and the northeast are dominated by cereals and oilseeds under cooler winters, warmer summers and deep arable soils, while Mediterranean departments in the south and along the lower Rhône favour vines, olives, fruit and open-field vegetables adapted to hot, dry summers and strong insolation. Mountain areas in the Alps, Pyrenees and Massif Central are characterised by extensive ruminant systems and hay-based fodder shaped by altitude, slopes and shorter growing seasons. These production patterns co-vary with France's main climate regimes—oceanic in the west, semi-continental in the northeast, Mediterranean in the south and mountain climates in higher- altitude areas—so that changes in weather and warming interact with very different farm calendars and biophysical constraints across departments. Episodes of extreme heat can slow or interrupt outdoor work, increase animal-care needs, compress seasonal windows in vineyards and horticulture, create bottlenecks for cereal harvest and haymaking, and tighten coordination along supply chains, and because these mechanisms load differently across OTEX systems, spatial heterogeneity in climate exposure translates into heterogeneous constraints on productivity.

2.2 Conceptual framework

The agricultural sector is known to exhibit strong nonlinear temperature effects. Burke et al. (2015) show a concave relationship between temperature and productivity for both agricultural and non-agricultural output, with moderate warming sometimes associated with gains and higher temperatures with sharp losses. Econometric and agronomic studies converge on the importance of thresholds (Lobell and Asseng, 2017). Schlenker and Roberts (2009) find that yields of major crops fall steeply once temperatures exceed critical levels, and Lobell et al. (2011) document similar nonlinear responses for maize in Africa with stronger losses under dry conditions. Subsequent work confirms that temperatures beyond roughly 29-32 °C are damaging for many crops and that extreme heat is a key driver of agricultural losses (Parent and Tardieu, 2012; D'Agostino and Schlenker, 2016; Butler et al., 2018).

Subnational studies for France fit into this broader picture and highlight spatial heterogeneity in climate sensitivity. van der Velde et al. (2012) relate soil moisture to maize and wheat yields over 2002-2007, Ceglar et al. (2016) use Partial Least Squares Regression on departmental data from 1989 to 2014 to quantify the influence of multiple environmental factors, and Gammans et al. (2017) estimate flexible temperature and precipitation response functions for wheat and barley and show robust negative effects of warming. Zampieri et al. (2017) attribute wheat yield anomalies to heat, drought and water excess and find substantial subnational variability. Schauberger et al. (2021) provide a longer-term view and report no historical increase in exposure-weighted vulnerability of French crop production to climatic hazards, even though sensitivity to weather remains strong. Event studies of the unforeseen 2016 wheat yield loss in France further underline how specific weather combinations can trigger extreme, spatially concentrated production shocks (Ben-Ari et al., 2018; Nóia Júnior et al., 2023). This body of work confirms that climate shocks affect French agriculture in a spatially heterogeneous way, but it focuses mainly on crop yields. As a result, it offers limited guidance on how extreme heat translates into departmental agricultural productivity, and it provides only a partial basis for targeting adaptation policies that operate at that scale.

Against this backdrop, we adopt a framework that makes threshold dynamics explicit and is suited to subnational productivity analysis. We define Extreme Degree Days (EDD) as cumulative degree-days above a critical threshold of 29 °C, in line with agronomic and economic evidence on damaging temperatures for major crops (Schlenker and Roberts, 2009; Parent and Tardieu, 2012; D'Agostino and Schlenker, 2016; Butler et al., 2018). EDD captures both the intensity and duration of extreme heat and provides a biologically grounded metric that can be linked to policy discussions on heat stress and adaptation planning. Our aggregate economic indicator that reflects how effectively inputs are combined is defined as value added per worker, a measure of agricultural labor productivity, following Olper et al. (2021).

This approach addresses two challenges highlighted in the literature. It extends the analysis of climate impacts beyond individual crops toward sector-wide performance and it does so at a spatially disaggregated scale that is directly relevant for French adaptation policy, allowing us to identify local vulnerabilities and heterogeneous responses to extreme heat in a way that national averages cannot reveal. Because the timing and intensity of these constraints depend on both local climate and the dominant production orientation, the same EDD shock can translate into very different disruptions to work organization and sectoral performance. Since these mechanisms load differently across OTEX systems, and hence across departments, we expect—and test for—heterogeneous dynamic responses of agricultural labor productivity at the departmental level.

3 Data and stylized facts

This section presents the two main datasets used in the analysis. The first combines high-resolution temperature records with a spatial inventory of land-use to construct a sector-specific indicator of extreme heat exposure. The second compiles departmental-level economic statistics on agricultural value added and employment, enabling a long-run subnational assessment of productivity trends in France's agricultural sector.

3.1 Measuring cumulative heat stress in French agriculture

To measure exposure to extreme temperatures, we use hourly 2-meter air temperature data from the ERA5-Land reanalysis dataset for mainland France, covering the years 1980-2023. The ERA5-Land dataset, produced by the Copernicus Climate Change Service, provides gridded temperature fields at a resolution of $0.1° \times 0.1°$ (Muñoz Sabater et al., 2019). Administrative boundaries for French departments are sourced from Eurostat's NUTS classification, enabling the assignment of each grid point to its corresponding department as depicted in Figure A1 (Appendix A.2).[1]

We construct an index of Extreme Degree Days (EDD) following Schlenker and Roberts (2009) and Lobell et al. (2011), integrating high-resolution temperature data with land-use information to restrict the measure to agricultural areas. The choice of 29 °C as the threshold is supported by agronomic and economic literature, which identifies temperatures above this level as particularly damaging for major crops (Schlenker and Roberts, 2009; Parent and Tardieu, 2012). Moreover, livestock are also susceptible to heat stress at comparable temperatures, leading to reduced productivity and adverse health outcomes (Rötter and Van de Geijn, 1999).

Coarse temperature indices (e.g., using daily maxima or averages) can obscure critical features of heat exposure, including the duration and intra-day dynamics of high temperatures. This can lead to systematic underestimation of the physiological and economic damage caused by extreme heat (Tack et al., 2015). To overcome these issues and compute EDD when only daily minimum and maximum temperatures are available (and not hourly temperatures), sinusoidal interpolation is used to estimate intra-day temperature profiles as in Schlenker and Roberts (2009) and Lobell et al. (2011). A key difference from these analyses is that we use hourly temperature data rather than a sinusoidal interpolation between minimum and maximum temperature. Although the use of hourly temperature data improves the accuracy of heat exposure measurements, differences between the two methods are generally modest. Nevertheless, hourly data provide a more precise characterization of extreme heat conditions affecting agricultural productivity.

For each grid cell j[2] and day d, the EDD is computed as:

[1] The departmental level in the NUTS classification is referred to as NUTS3 level.

[2] $j \in J$, J being the set of all grid points and the number of grid points.

$$\mathrm{EDD}_{j,d} = \sum_{h=1}^{24} \max(0, T_{j,h,d} - T^*) \times \frac{1}{24} \tag{1}$$

where $T_{j,h,d}$ is the temperature at grid cell j, hour h of day d, and $T^* = 29$ °C is the physiological threshold. The factor 1/24 converts cumulative "degree-hours" into "degree-days", so one unit of EDD equals 24 degree-hours above 29 °C. Intuitively, it rises with both the intensity (how far temperatures exceed 29 °C) and the duration (how many hours they do so).

Daily values are summed to obtain an annual total:

$$\mathrm{EDD}_{j,t} = \sum_{d \in D_t} \mathrm{EDD}_{j,d} \tag{2}$$

where $\mathrm{EDD}_{j,t}$ is the total annual exposure to extreme heat at grid point j for year t and D_t is the set of all days in year t.

3.2 A spatially weighted measure of extreme heat exposure

Because climate impacts on agriculture arise from localized exposure where production actually occurs, we integrate land-use information to compute a agriculture-specific EDD measure.

We associate each grid point (j) with its corresponding administrative unit at the NUTS3 (departmental) level based on Eurostat boundaries,[3] as depicted in Figure A1 (Appendix A.2). This spatial matching allows grid-level observations to be systematically aggregated into department-level measures, providing a consistent framework for computing EDD at the departmental scale. Figure 2 illustrates this process using data from the year 2023.

Because extreme temperature affect agriculture primarily through localized impacts—directly where crops or livestock are located—we combine the EDD index with spatial land-use data from the CORINE Land Cover (CLC) database. CLC is a harmonized biophysical land cover dataset derived from satellite imagery. It is generated through visual interpretation of high-resolution images, with a spatial accuracy of approximately 20 meters. The dataset delineates homogeneous land-use units with a minimum mapping unit of 25 hectares. Available census years include 1990, 2000, 2006, 2012, and 2018.

[3]The list of all NUTS3 departments is provided in Table A1 (Appendix A.1).

Figure 2: Annual EDD values for 2023 in three departments

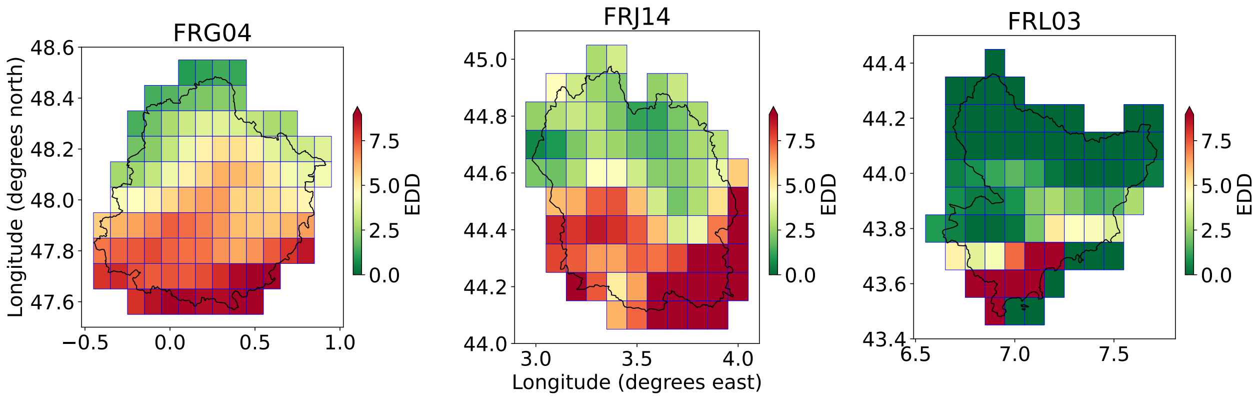

Note: The figure shows grid-level Extreme Degree Days (EDD) for 2023 for three departments: FRG04 (Sarthe, left), FRJ14 (Lozère, center), and FRL03 (Alpes-Maritimes, right). Each grid cell represents the annual EDD at that location. Values above the 90th percentile are truncated to improve visual contrast. *Sources*: ERA5-Land.

This dataset provides a consistent classification of land-use types. For the analysis, we rely on the first hierarchical level, which distinguishes five broad categories: built-up areas, agricultural land, forests and semi-natural environments, wetlands, and water surfaces. Figure 3 provides an illustration of this decomposition for a selected year and region.

Figure 3: Example of 2018 CORINE Land Cover (CLC) classification

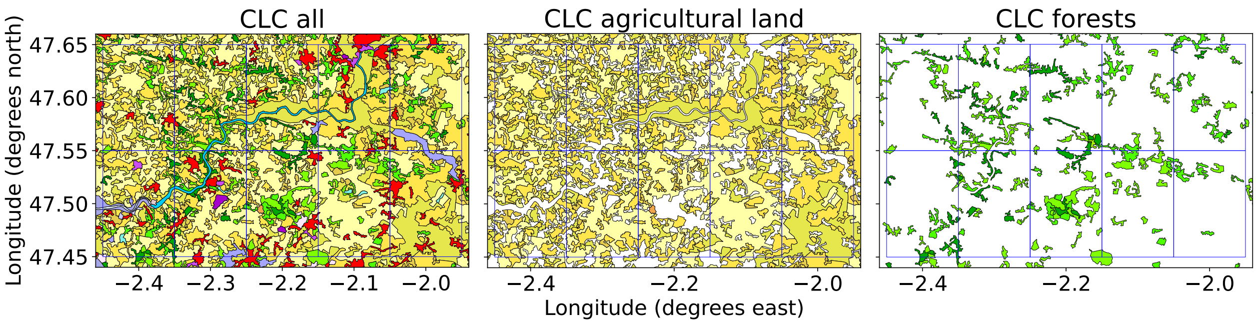

Note: Illustration of land-use decomposition based on the 2018 CORINE Land Cover (CLC) census. The three panels show all land-use types (left), agricultural land (center), and forest and semi-natural areas (right). Grid overlays correspond to ERA5-Land grid points. The mapped area is located near the Vilaine estuary. A detailed legend of land-use classifications is provided in Figure A2 (Appendix A.2). *Sources*: ERA5-Land and CORINE Land Cover.

We restrict our analysis to agricultural land and for each department, we delineate the complete extent of agricultural areas. The resulting map in Figure 4 reveals substantial heterogeneity, both across and within regions. These spatial disparities underscore the importance of employing a sector-specific metric when assessing the impact of extreme temperatures on agriculture.

Figure 4: Agricultural land cover in 2018 for three selected departments

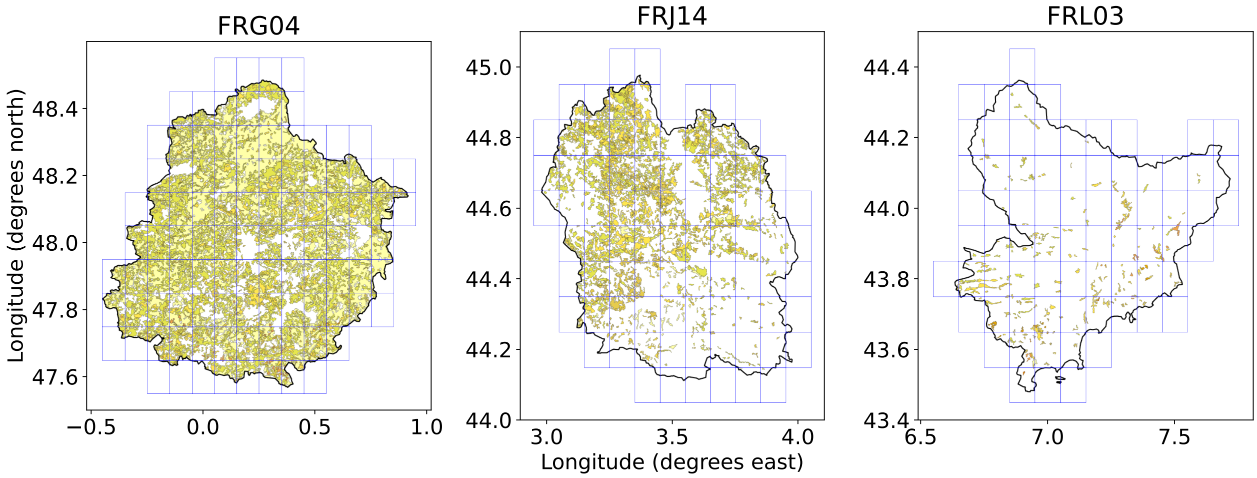

Note: Agricultural land cover in three departments based on the 2018 CLC census. Grid overlays correspond to ERA5-Land grid points. White areas indicate land not classified as agricultural land. *Sources*: ERA5-Land and CORINE Land Cover.

Based on this classification, we compute the relative share of agricultural land within each grid cell, expressed as a proportion of the department's total agricultural area. This procedure identifies grid cells where agricultural activity is most concentrated. For each grid cell j we obtain five values corresponding to the five available CLC census years.

We divide the dataset into five subperiods—1980-1996, 1997-2003, 2004-2009, 2010-2015, and 2016-2023—matching the CLC census years of 1990, 2000, 2006, 2012, and 2018, respectively. Thus, we obtain a share weight w_{j_r} for each grid cell j in department r, reflecting the spatial distribution of agricultural land. Figure 5 illustrates this distribution for selected departments.

Figure 5: Share of agricultural land per grid cell in 2018 for three departments

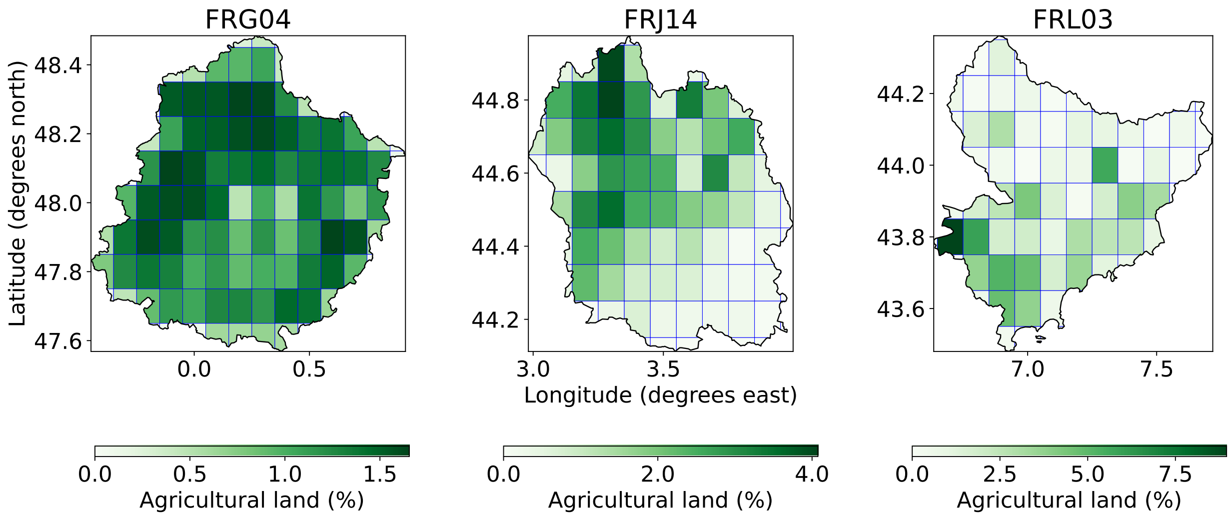

Note: Share of agricultural land per grid cell in three departments, based on the 2018 CLC census. Values represent the percentage of each department's total agricultural area and are used for the period 2016–2023. Grid overlays correspond to ERA5-Land grid cell. *Sources*: ERA5-Land and CORINE Land Cover.

The annual sector-specific EDD for department r in year t, denoted $\text{EDD}_{r,t}$, is defined as:

$$\text{EDD}_{r,t} = \sum_{j_r=1}^{J_r} w_{j_r} \text{EDD}_{j_r,t} \ , \tag{3}$$

where J_r is the set of grid points within department r. Weights $w_{j_r} \in [0;1]$ and $\sum_{j_r=1}^{J_r} w_{j_r} = 1$. This weighting scheme ensures that the EDD index reflects only heat exposure affecting agricultural land, thus reducing measurement error by excluding irrelevant land types.

Figure 6 and Figure 7 present the monthly distribution and geographical evolution of EDD across French departments. Along with Figure A3 and Figure A4 (Appendix A.2), these figures document an upward shift in the entire distribution of heat exposure, daily, monthly and annually, consistent with broader climate change trends. The observed spatial heterogeneity highlights the importance of using disaggregated, land-use–adjusted climate indicators when assessing agricultural impacts.

Figure 6: Monthly sector-specific EDD evolution for France, 1980–2023

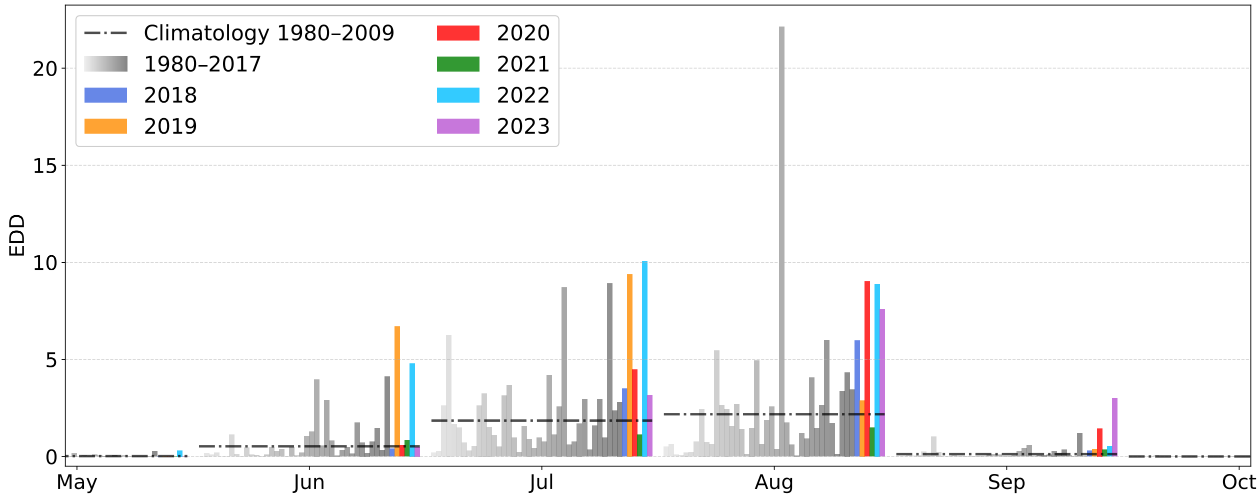

Note: Monthly sector-specific EDD evolution for France over 1980-2023, averaged nationally. The series is constructed from high-resolution ERA5-Land reanalysis data, combined with CORINE Land Cover to isolate agricultural land. The chart shows, for each month, the evolution for the 1980-2017 period (gray gradient), the last six years (diverse colors), and the climatological mean of the 1980-2009 period (black dashed line). Other months have no EDD. *Sources*: ERA5-Land and CORINE Land Cover.

Figure 7: Geographical distribution of annual average sector-specific EDD by department

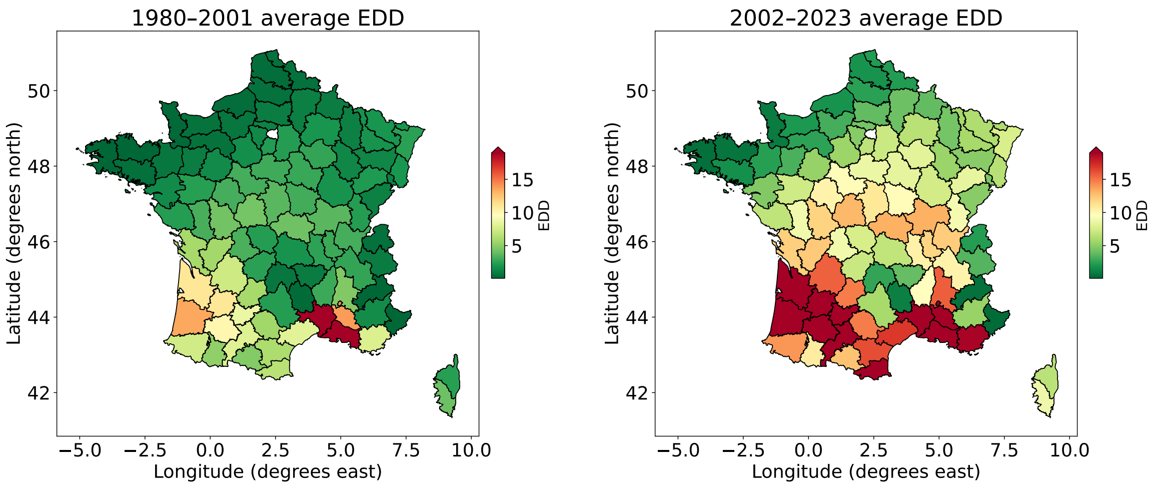

Note: Annual average sector-specific Extreme Degree Days (EDD) by department for two periods—1980-2001 (left) and 2002-2023 (right). The estimates are constructed from high-resolution ERA5-Land reanalysis data combined with CORINE Land Cover to isolate agricultural land. High values are truncated at the 90th percentile to enhance visual contrast. *Sources*: ERA5-Land and CORINE Land Cover.

3.3 Agricultural productivity

Following Olper et al. (2021), our economic analysis focuses on the value added per worker in the agricultural sector—hereafter referred to as agricultural productivity—using data from the European Commission's ARDECO database. This database provides detailed economic indicators disaggregated to the NUTS3 (departmental) level, allowing for a granular assessment of agricultural performance across mainland France. It spans the period 1980-2023 at annual frequency, enabling a long-term perspective on both productivity levels and growth trends. For each department r and year t, we denote log real agricultural productivity as $y^a_{r,t}$.

Figure 8 presents both the average productivity levels and the average annual growth rates (AAGR) of agricultural productivity over the 1980-2023 period and Figure 1 shows the main technical and economic organization of farms (OTEX) for each department.[4] The results reveal substantial spatial disparities. The highest productivity levels are observed in the northern regions, along parts of the coastal zones, and in selected areas of Grand Est and Bourgogne-Franche-Comté. Notably, Marne stands out as the most productive department, largely due to its specialization in champagne production. Similarly, departments specialized in wine production, such as Gironde and Var, also record above-average productivity

Figure 8: Agricultural productivity levels and growth rates, 1980-2023

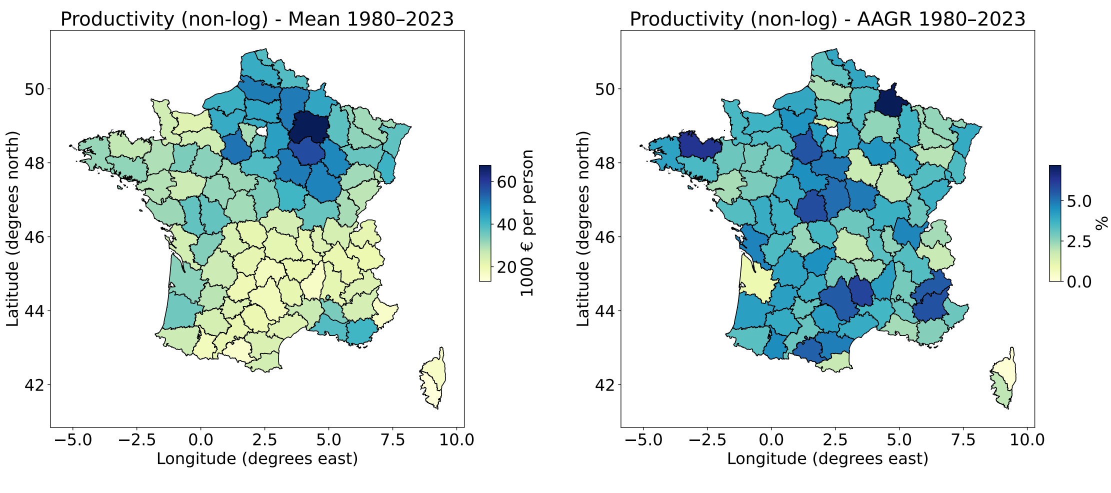

Note: Average agricultural productivity (value added per worker) by department for 1980-2023 (left). Average annual growth rate of agricultural productivity over the same period (right). No log transformation applied. *Sources*: ARDECO.

Figure 1 highlights both the persistence and gradual shifts in agricultural specialization. In

[4]Figures A5 and A6 (Appendix A.2) also display main and secondary OTEX for 2010 and 2020 respectively.

2010, northern departments were largely dominated by cereals and other field crops, while viticulture was concentrated in the southwest, Burgundy, and parts of the Mediterranean coast. By 2020, these broad patterns remained, but some departments saw changes in dominant activities, with a gradual expansion of mixed livestock systems and adjustments in wine-growing areas. Southern inland departments remain heavily oriented toward livestock farming—beef, dairy, and sheep—whereas horticulture and permanent crops appear in localized pockets.

This spatial organization of production reflects the productivity disparities documented above. Departments specialized in cereals and viticulture generally maintain higher productivity levels, reflecting scale economies and higher value-added, while livestock-oriented departments tend to show lower productivity. The persistence of these patterns over time also coincides with the regional clusters of weaker productivity growth—particularly in Bourgogne–Franche-Comté, Auvergne–Rhône-Alpes, and the latitude corridor between 44.5° and 46° north—where structural reliance on livestock farming leaves agriculture more exposed to climate stress and slower to adopt productivity-enhancing technologies.

4 Empirical strategy

This section details the econometric strategy used to assess the causal impact of extreme heat exposure on agricultural productivity. Our approach relies on the local projection (LP) method introduced by Jordà (2005), enhanced by the unit-specific estimation framework proposed by Berg et al. (2024) to address slope heterogeneity across French departments (NUTS3 level). This framework is particularly appropriate for analyzing climate–economy dynamics because it allows responses to be traced over different time horizons while accommodating cross-departmental variation in sensitivity to temperature shocks.

The rationale for this approach stems from two considerations. First, agricultural responses to extreme temperatures are likely nonlinear, heterogeneous across locations, influenced by production systems, and may persist over multiple years. Second, standard panel regressions often impose homogeneity restrictions, assuming a common response across units. Such restrictions may bias inference and obscure important local dynamics. This is particularly problematic in the France-specific agricultural context, where departments differ widely in economic and climatic baselines, crop/livestock specialization, infrastructure, and adaptive capacity.

Panel regressions such as Dell et al. (2012), Burke et al. (2015), and Kahn et al. (2021) typically constrain regional heterogeneity by allowing at most a limited set of interactions (e.g., income or agro-ecological zones). However, recent work by Berg et al. (2024) highlights that these specifications often fail to capture substantial subnational variation, particularly when climate shocks are spatially uneven and adaptation trajectories differ across regions. By estimating local impulse-response functions separately for each department, we allow both the the magnitude and persistence of climate impacts to vary without imposing functional restrictions.

4.1 Local projections framework

We estimate the dynamic effects of extreme heat exposure—measured via our sector-specific EDD index—on agricultural productivity using the following equation, estimated separately for each department r and forecast horizon $h \in \{0, \ldots, 5\}$:

$$100 \cdot (y^a_{r,t+h} - y^a_{r,t-1}) = \beta_{r,h}\mathrm{EDD}_{r,t} + \mathbf{X}'_{r,t,h}\phi_{r,h} + \epsilon_{r,t+h} \ , \tag{4}$$

where $100 \cdot (y^a_{r,t+h} - y^a_{r,t-1})$ represents one hundred times the change in log real agricultural productivity between $t-1$ and $t+h$, $\mathrm{EDD}_{r,t}$ is the annual, sector-weighted Extreme Degree Days (EDD) measure for department r, $\mathbf{X}'_{r,t,h}\phi_{r,h}$ is a vector including a constant and lagged control variables, and $\epsilon_{r,t+h}$ is an error term.

This specification estimates the cumulative change in productivity between $t-1$ and $t+h$ as a function of the EDD in year t, while controlling for prior productivity dynamics. The control vector $\mathbf{X}'_{r,t,h}\phi_{r,h}$ is defined as:

$$\mathbf{X}'_{r,t,h}\phi_{r,h} = \sum_{p=1}^{P} \beta_{r,h,p} 100 \cdot (y^a_{r,t+h-p} - y^a_{r,t-1-p}) + \sum_{q=1}^{Q} \beta_{r,h,q}\mathrm{EDD}_{r,t-q} + \mu_{r,h} \ , \tag{5}$$

where, P and Q denote the lag lengths for productivity differences and EDD shocks, selected via the Akaike Information Criterion (AIC) at each horizon h. The inclusion of lagged temperature effects captures delayed effects from past temperature shocks, a feature emphasized in previous climate-economy studies (Dell et al., 2012; Berg et al., 2024).

Estimation proceeds in three steps. First, for each department and forecast horizon h, we select the optimal lag lengths P and Q using the AIC. Second, we estimate Equation (4) using Ordinary Least Squares (OLS) and compute Newey-West standard errors, which are robust to both heteroskedasticity and autocorrelation (Jordà, 2005). Third, we recover the sequence of coefficients $\beta_{r,h}$ ($h \in \{0, \ldots, 5\}$), which we use to construct impulse-response functions (IRFs) for each department. These IRFs depict the dynamic response of agricultural productivity to a one-unit increase in extreme temperature exposure, allowing us to assess whether the effects are immediate, persistent, or lagged, and how their magnitude varies across departments.

4.2 Testing for slope homogeneity

To assess whether productivity responses to EDD differ across departments, we test the null hypothesis of slope homogeneity—that is, the assumption that all departments respond to extreme heat in the same way. While this restriction is standard in panel regressions, it can conceal meaningful cross-regional variation in climate sensitivity, production structures, and adaptive capacity.

Under the homogeneity assumption, the coefficient on EDD in the local projection framework is constrained to be identical across departments. Rejecting this assumption provides statistical justification for estimating department-specific impulse-response functions (IRFs), as estimated in Section 4.1.

We first estimate Equation (6) for each department separately at horizon $h = 0$, which captures the contemporaneous response of productivity to EDD:

$$100 \cdot (y^a_{r,t} - y^a_{r,t-1}) = \beta_{r,0} EDD_t + \mathbf{X}'_{r,t,0}\phi_{r,0} + \epsilon_{r,t} \ . \tag{6}$$

We then classify departments into two groups based on the sign of $\beta_{r,0}$. To test for systematic differences, we estimate a constrained pooled regression with interaction terms defined by the sign of $\beta_{r,0}$:

$$100 \cdot (y^a_{r,t} - y^a_{r,t-1}) = \beta^+_{r,0} \cdot \mathrm{EDD}_{r,t} \cdot \mathbb{1}\{\beta_{r,0} > 0\} + \beta^-_{r,0} \cdot \mathrm{EDD}_{r,t} \cdot \mathbb{1}\{\beta_{r,0} < 0\} + X'_{r,t,0}\phi_{r,0} + \epsilon_{r,t} \tag{7}$$

where coefficients on the control variables are allowed to vary across departments.

We test $H_0 : \beta^+_{r,0} = \beta^-_{r,0}$ using a Wald test. The null is strongly rejected ($p < 0.001$), providing robust evidence that EDD impacts are not homogeneous across departments. This result provides clear justification for department-specific estimation and demonstrates the importance of relaxing slope homogeneity in climate–agriculture models. It also extend the findings of Berg et al. (2024) to a subnational agricultural setting.

5 Results

This section presents the main findings of our empirical analysis on the impact of sector-specific Extreme Degree Days (EDD) on agricultural productivity in France. We proceed in three steps. First, we estimate department-level impulse-responses using local projections, plot the distribution of responses, and map their spatial patterns. Second, we compare the performance of our sector-specific EDD metric across alternative temperature thresholds. Third, we conduct a set of robustness checks.

5.1 Department-level productivity responses to sector-specific EDD

We begin by estimating the dynamic response of changes in agricultural productivity to extreme heat exposure using the local projections framework introduced in Section 4.[5] Figure 9 reports the distribution of estimated coefficients $\beta_{r,h}$ for forecast horizons $h \in \{0, \ldots, 5\}$.

Results show that increases in sector-specific EDD lead to statistically significant and economically meaningful reductions in agricultural productivity. Negative effects emerge immediately (at $h = 0$), remain in the short term ($h = 1$ and $h = 2$) and intensify at medium horizons ($h = 3$ and $h = 4$) indicating persistent damage from temperature shocks. The adverse impacts begin to attenuate at longer horizons (particularly by $h = 5$), yet they remain prevalent across most departments, suggesting limited adaptive capacity in the agricultural sector. These findings contrast with national-level evidence, such as Berg et al. (2024), who report no significant response of aggregate GDP to extreme temperature exposure in France. By applying a sector-specific and spatially disaggregated framework, our analysis reveals substantial and heterogeneous impacts that are masked in aggregate studies.

[5] The department-level impulse-response functions (IRFs) are presented in Figure A7 (Appendix A.2).

Figure 9: Distribution of estimated departmental impacts $\beta_{r,h}$ of sector-specific EDD

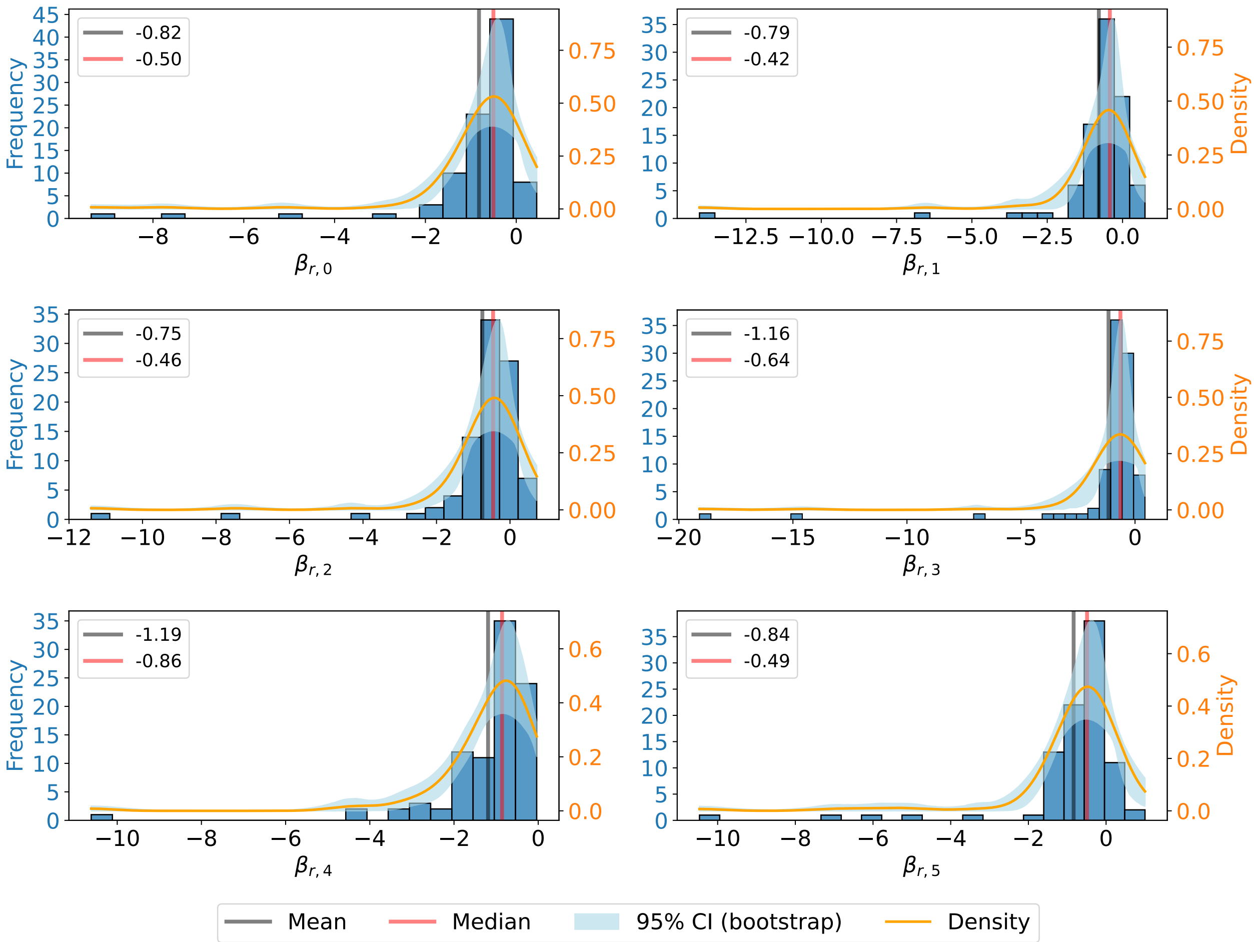

Note: This figure displays the distribution of estimated coefficients $\beta_{r,h}$ from the local projection regressions across six forecast horizons $h \in \{0, \dots, 5\}$. For each horizon, bar charts depict the frequency of coefficient estimates (left axis), while kernel density curves (solid orange lines, right axis) depict the smoothed distribution. The vertical grey line indicates the mean, and the red line denotes the median of the estimates. Light blue shading indicates the 95% confidence band of the density estimate, obtained via bootstrapping. *Sources*: ERA5-Land, ARDECO, and CORINE Land Cover.

Figure 10 provides a detailed characterization of the distribution of department-level responses $\beta_{r,h}$ to sector-specific EDD across the forecast horizons. The combination of kernel densities, scatter plots, and box-and-whisker diagrams reveals that the majority of estimated coefficients are negative at each horizon, supporting the hypothesis that extreme heat systematically depresses agricultural productivity.

The distribution also exhibits increasing dispersion over longer horizons, suggesting that the variability of responses across space increases over time. This widening spread likely reflects both structural heterogeneity in agro-climatic conditions and production systems across departments, and rising uncertainty regarding long-run adaptation or exposure pathways. These results underscore the importance of allowing for unit-specific dynamics in climate-economy analyses, since imposing uniform responses would obscure substantial regional heterogeneity.

Figure 10: Distributional patterns of estimated coefficients $\beta_{r,h}$ across forecast horizons

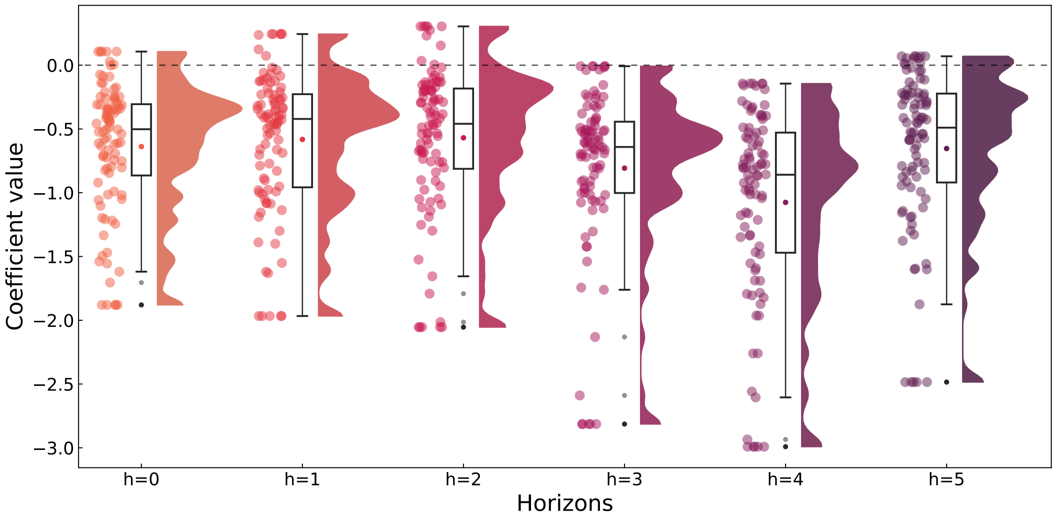

Note: The figure displays the distribution of estimated coefficients $\beta_{r,h}$ from Equation (4), associated with sector-specific EDD, across forecast horizons $h \in \{0, \ldots, 5\}$. Each panel corresponds to a horizon and is color-coded accordingly. The scatter plots show the raw coefficient values at the departmental level. Superimposed on each panel are box-and-whisker plots, in which the black horizontal line indicates the median, and the colored dot marks the mean. The whiskers extend to 1.5 times the interquartile range, with outliers shown as gray points. Smoothed kernel density estimates (Gaussian kernels) illustrate the overall distribution shape. The data are winsorized. *Sources*: ERA5-Land, ARDECO, and CORINE Land Cover.

Figure 11 maps the geographical distribution of the estimated responses $\beta_{r,h}$ across French departments for horizons $h = 0$ to $h = 5$. At short horizons, negative effects cluster notably in southern and central regions, including Corsica, where agricultural systems are particularly exposed to heat stress. By horizon $h = 3$, significant negative responses extend across a wider set of departments, indicating increasing persistence and spatial diffusion of climate-related damage. A clear north-south gradient emerges at several horizons, with departments in the north and west generally less affected, although local pockets of high vulnerability persist throughout the country, especially for horizons $h = 3$ and $h = 4$.

Figure 11: Spatial distribution and significance of estimated EDD impacts $\beta_{r,h}$ by horizon

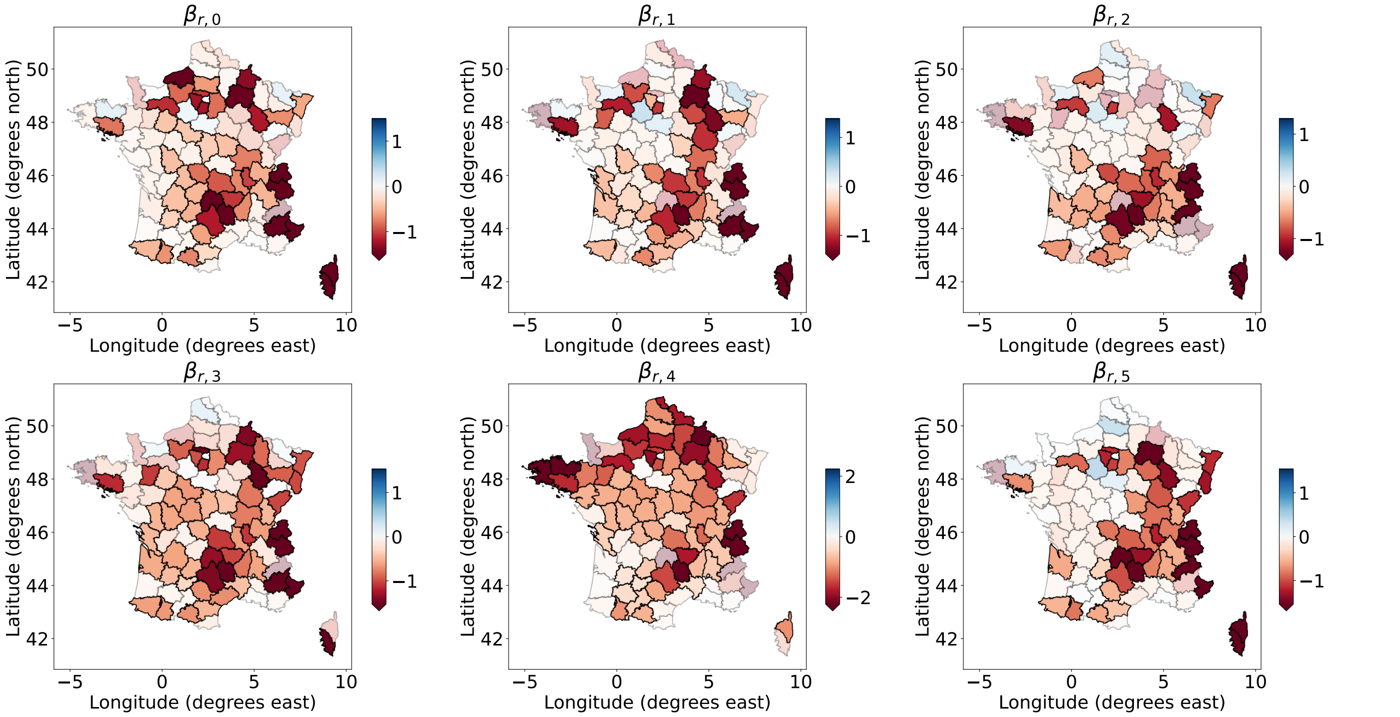

Note: Each panel shows the departmental-level coefficient $\beta_{r,h}$ estimated from the local projection model in Equation (4), corresponding to a forecast horizon $h \in \{0, \dots, 5\}$. Shading intensity reflects the magnitude and direction of the estimated effect. Red hues indicate negative impacts and blue hues indicate positive impacts. Statistically significant coefficients are shown in opaque colors, while transparent areas indicate non-significance. Color scales vary by panel to accommodate differences in magnitude. Extreme values are truncated for legibility. *Sources*: ERA5-Land, ARDECO, and CORINE Land Cover.

Table 1 reinforces the evidence presented in Figures 9, 10, and 11 by providing a numerical breakdown of the estimated coefficients. Across all horizons, between 81 and 92 out of 92 departments display negative point estimates, indicating a remarkably consistent pattern across space. Moreover, no department exhibits a statistically significant positive effect at any horizon. The number of statistically significant negative coefficients increases with the projection horizon, peaking at 55 departments at $h = 3$ and 64 at $h = 4$, before declining at $h = 5$. Even at shorter horizons, at least 35 departments display significant negative responses. These figures highlight both the breadth and the persistence of the adverse impact of extreme heat exposure on agricultural productivity, and underscore the systematic nature of the vulnerability documented in the spatial analysis.

Table 1: Summary of estimated effects $\beta_{r,h}$ of sector-specific EDD on agricultural productivity

h	$\beta_{r,h}$_coef_pos	$\beta_{r,h}$_coef_neg	$\beta_{r,h}$_sign_counts	$\beta_{r,h}$_sign_pos	$\beta_{r,h}$_sign_neg
0	7	85	47	0	47
1	8	84	41	0	41
2	10	82	35	0	35
3	5	87	55	0	55
4	0	92	64	0	64
5	11	81	41	0	41

Note: For each forecast horizon h, the table reports the count of departments with positive and negative estimated coefficients $\beta_{r,h}$, as well as the number that are statistically significant at the 5% level. Columns labeled "sign_pos" and "sign_neg" denote departments with significant positive and significant negative effects, respectively. The estimates are derived from Equation (4) using local projections with Newey-West standard errors. *Sources*: ERA5-Land, ARDECO, CORINE Land Cover, author's computations.

5.2 Sensitivity analysis: threshold variation for EDD calculation

Our analysis focuses on a single threshold (29 °C) because it is widely cited in the literature as relevant for several major crops. However, agronomic studies show that crops differ in their heat tolerance thresholds (Hatfield et al., 2011; Parent and Tardieu, 2012). To ensure that our results are not driven by the choice of a single cutoff, we conduct a sensitivity analysis using alternative thresholds.

Specifically, we reprocess the EDD measure using thresholds of 23 °C, 26 °C, and 32 °C and re-estimate Equation (4). The lower bound of 23 °C does not correspond to a sharp physiological damage threshold but allows us to assess whether moderate heat exposure already generates economically measurable effects. In contrast, the higher threshold of 32 °C isolates more severe heat episodes and tests whether the estimated impacts are driven primarily by rare and extreme events.

These alternative thresholds allow us to evaluate the stability of the estimated responses across different segments of the temperature distribution and to assess whether the nonlinear relationship between temperature and productivity is sensitive to the definition of extreme exposure. We define them using:

$$\mathrm{EDD}^{\sigma}_{r,t} = \frac{1}{J_r} \sum_{j_r=1}^{J_r} \mathrm{EDD}_{j_r,t} \ , \tag{8}$$

where $\mathrm{EDD}^{\sigma}_{r,t} \in \{\mathrm{EDD}^{23}_{r,t},\ \mathrm{EDD}^{26}_{r,t},\ \mathrm{EDD}^{32}_{r,t}\}$ captures exposure to heat exceeding 23 °C, 26 °C, and 32 °C respectively. The baseline measure corresponds to $\mathrm{EDD}^{29}_{r,t}$.

By replacing the EDD measurement calculated at the 29 °C threshold, $\text{EDD}_{r,t}$, with those at alternative thresholds, $\text{EDD}^{\sigma}_{r,t}$, into the local projection framework, the baseline specification becomes:

$$100 \cdot (y^a_{r,t+h} - y^a_{r,t-1}) = \beta^{\sigma}_{r,h}\text{EDD}^{\sigma}_{r,t} + \mathbf{X}'_{r,t,h}\phi_{r,h} + \epsilon_{r,t+h} \ , \tag{9}$$

We then obtain coefficient estimates $\beta^{\sigma}_{r,h}$ in parallel with our main estimates $\beta_{r,h}$ and compare them across horizons. Results of this analysis are shown in Figure 12. The negative impact of EDD on agricultural productivity becomes larger as the threshold increases, and this effect is accompanied by greater heterogeneity in responses. In particular, the $\text{EDD}^{32}_{r,t}$ measure shows pronounced negative effects, underscoring the severe productivity losses associated with exposure to very high temperatures. However, the overall effect remains similar, with a persistent negative impact of EDD on agricultural productivity and merely limited attenuation.

Figure 12: Sensitivity analysis based on threshold variations, comparison between $\beta_{r,h}$ and $\beta^{\sigma}_{r,h}$

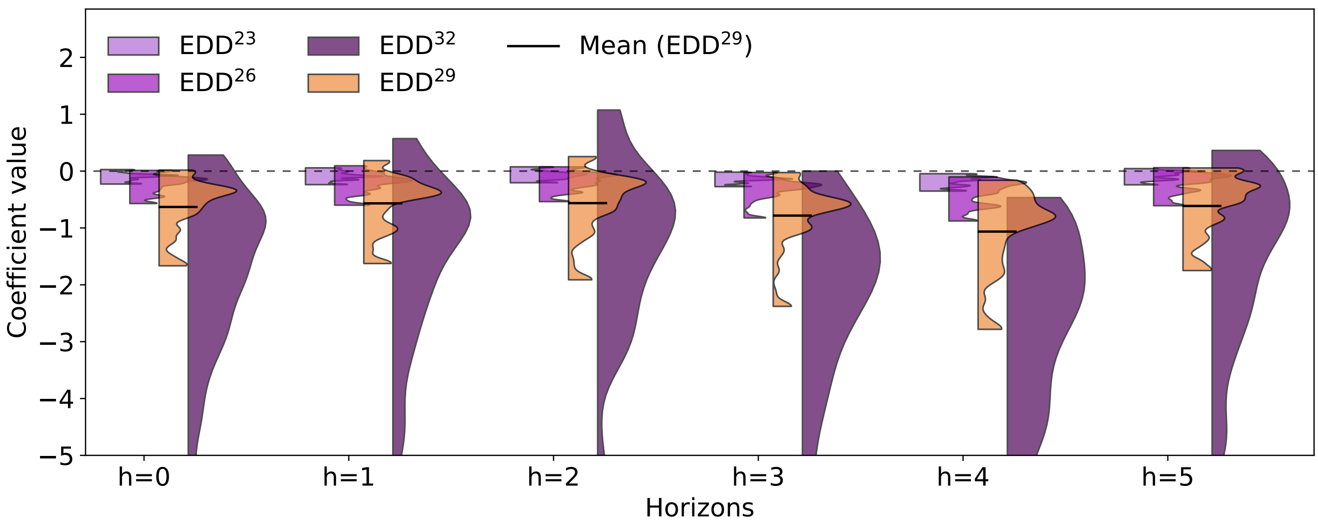

Note: For each horizon we present the distributions of estimate derived from equations (4) for different EDD thresholds. The distribution of baseline threshold (29 °C) coefficients $\beta_{r,h}$ is shown in orange and distributions of alternative threshold (23 °C, 26 °C and 32 °C) coefficients $\beta^{\sigma}_{r,h}$ are shades of purple. The baseline mean estimate is indicated with a black line in the distribution associated with the threshold of 29 °C. Data are winsorized. Low values are truncated to improve visual. *Sources*: ERA5-Land, ARDECO, and CORINE Land Cover.

5.3 Robustness checks

We conduct a set of robustness checks based on alternative specifications of Equation 4, specifically by including additional controls to mitigate omitted variable bias—even though our baseline approach partially addresses this issue. We compare the distribution of estimates across specifications to ensure that the inclusion of these controls does not affect our core results.

Our control specifications involve estimating Equation 4 under nine variations, each incorporating different combinations of four control variables to assess robustness. Among these, precipitation is included due to its critical role in shaping both agricultural productivity and broader economic activity. Several studies, such as Burke and Tanutama (2019) and Damania et al. (2020), emphasize its importance for aggregate production—particularly in regions where agriculture is a major economic driver. Similarly, Deschênes and Greenstone (2007) identify precipitation as a primary determinant of agricultural output, directly affecting crop yields, water availability, and related sectors. To capture this influence, we include the annual mean of daily precipitation at the departmental level, obtained from the ERA5-Land database.

We also control for public spending in each department to account for variations in government investment and administrative capacity across regions. Differences in public spending can influence economic outcomes through better infrastructure, the quality of public services, and the provision of targeted assistance programs. These factors can enhance productivity, economic resilience, and a region's ability to respond to external shocks. To proxy for this dimension, we include public administration value added per capita, constructed from Eurostat population data and value-added data from the ARDECO database.

To account for the potential influence of a department's economic weight within its region, or differential responses to temperature shocks based on regional importance, we include a control for departmental economic influence. This variable is defined as the share of a department's total value added (across all sectors) in regional total value added.

Finally, we control for the share of the market sector in the economy, to account for potential spillover effects from a growing or declining market sector. This variable is defined as the ratio of market-sector value added to total value added and is also sourced from the ARDECO database.

From these four control variables, we construct nine alternative specifications of equation 4. Four include each control individually, while the remaining five combine multiple controls. To ensure these combinations do not introduce multicollinearity, we retain only those with Variance

Inflation Factors (VIFs) below conventional thresholds. Table 2 summarizes the control specifications and the variables included.

Table 2: Summary of variables included in each control specification

Variable	Name	1	2	3	4	5	6	7	8	9
Public spending per capita	admin	x					x	x		x
Regional influence of the department	influence		x			x	x			x
Average annual daily precipitation	rain			x		x		x	x	x
Share of the market sector	marketVA				x				x	

Note: : This table lists the variables included in each of the nine control specifications. Columns 1–9 correspond to the respective specifications. An "x" indicates that the variable is included. For simplicity, we refer to the specifications by number.

To avoid presenting all the distributions and geographical maps associated with these specifications, we summarize results in Tables A2 and A3 (Appendix A.1). Table A2 reports findings for all $\beta_{r,h}$, while Table A3 focuses only on statistically significant $\beta_{r,h}$ estimates. We conduct two statistical tests to compare distributions: the Kolmogorov-Smirnov (KS) test and the Mann-Whitney U (MWU) test. The KS test assesses whether the distribution of estimates under the control specification differs from that of the baseline, while the MWU test evaluates whether the samples originate from identical distributions.

We find that the null hypothesis is rejected for both tests at horizon 3 for control specifications 1, 2, 4, and 6, and at horizon 4 for specifications 1 and 9. These rejections suggest statistically significant differences in the distribution of estimates in these cases. However, at horizons 0 to 2 and horizon 5, we do not reject the null hypothesis for both tests, indicating stability in the results at shorter and longer horizons. Moreover, when the comparison is restricted to statistically significant $\beta_{r,h}$ estimates, we never reject the null hypothesis for both tests across any horizon or specification. These findings underscore the robustness of our estimates, even when additional controls are introduced. Overall, the results reinforce the validity of our baseline approach in capturing the fundamental relationships between extreme heat and agricultural productivity.

5.4 Robustness to humidity-adjusted heat exposure

As an additional robustness check, we construct an alternative measure of extreme heat exposure that accounts for atmospheric humidity. Specifically, we compute wet-bulb temperature using 2-meter air temperature and 2-meter dew point data from ERA5-Land, and define an Extreme

Degree Days measure based on humidity-adjusted temperature. To ensure comparability with our baseline specification, the wet-bulb threshold is calibrated so that the national frequency of exceedance matches that of the 29 °C dry-bulb threshold over the full sample period (1980-2023). Re-estimating the local projections with this humidity-adjusted indicator yields qualitatively similar spatial patterns and dynamic responses. While statistical significance is somewhat reduced at horizons $h = 2$ and $h = 5$, the remaining horizons display effects that are very close to the baseline estimates. Spatially, the strongest impacts remain concentrated in the inland corridor between 44.5° and 46° north latitude. Effects appear less pronounced in western departments, whereas northern areas exhibit comparatively stronger responses under the humidity-adjusted specification. Overall, the geographic distribution and sign of the responses remain consistent with the baseline specification. Detailed construction, estimation results, and discussion are reported in Appendix A.3.

6 Discussion and conclusion

This paper combines ERA5-Land reanalysis data with high-resolution CORINE Land Cover information to construct a sector-specific measure of Extreme Degree Days (EDD) at the subnational level in France. By weighting extreme heat exposure by agricultural land use, we capture substantial spatial heterogeneity in thermal stress while maintaining a parsimonious and spatially consistent indicator. This approach aligns with a growing literature that emphasizes nonlinear temperature effects in climate-economy relationships while relying on aggregated exposure metrics (Dell et al., 2014; Burke et al., 2015; Hsiang, 2016).

Methodologically, we extend the local projection framework proposed by Berg et al. (2024) to the agricultural sector at the departmental level and build on Olper et al. (2021) by introducing a sector-specific measure of extreme temperatures. Using data collected between 1980 and 2023, we produce geographically disaggregated estimates specific to each department concerning the dynamic effects of heat exposure on agricultural labor productivity, allowing for spatial heterogeneity to be taken into account.

From an economic perspective, our results indicate that increases in EDD exert a significant and persistent negative impact on agricultural labor productivity. The effects materialize immediately ($h = 0$), persist in the short run ($h = 1$ and $h = 2$), and intensify at medium horizons ($h = 3$ and $h = 4$), with only limited attenuation at $h = 5$. Spatially, productivity losses are concentrated in central and southern France, as well as in parts of the north. Several livestock-oriented and relatively low-productivity departments exhibit stronger and more persistent negative responses, forming a corridor of heightened vulnerability roughly between 44.5° and 46° north latitude. These findings are robust to alternative EDD thresholds and to a range of control specifications and distributional tests, consistent with earlier evidence on heterogeneous climate impacts in agriculture (Burke et al., 2015; Olper et al., 2021).

While our results highlight economically meaningful patterns of vulnerability, they should be interpreted in light of several limitations. First, from an agronomic perspective, agricultural productivity is shaped by a wide set of agro-climatic factors, including precipitation, soil moisture, solar radiation, wind, and their interactions with crop physiology and phenological stages. Our analysis deliberately abstracts from this multidimensionality by focusing on extreme heat exposure as a synthetic indicator. This choice reflects our objective to estimate an aggregate economic response to extreme temperatures at a spatial scale where detailed crop- or stage-specific modeling such as that used in gridded crop models (Rosenzweig et al., 2014) is infeasible and where multiple production systems coexist.

Second, the EDD measure is based on air temperature and does not explicitly account for atmospheric humidity, which can amplify heat stress for crops, livestock, and agricultural workers. Temperature-adjusted indicators incorporating humidity, such as wet-bulb temperature or related heat stress indices, are often used in agronomic and occupational health studies to capture these mechanisms more directly. However, their rigorous construction typically requires additional information (e.g., radiation and wind) that is not consistently available at the temporal and spatial resolution considered here. We therefore prioritize a homogeneous and directly observable measure of extreme heat, in line with much of the empirical climate-economics literature (Dell et al., 2014). Using an approximation, supplementary analysis explore an alternative temperature-based indicator adjusted for humidity to assess the robustness of our findings in Appendix A.3.

Third, our empirical framework relies on an aggregate measure of extreme heat exposure, constructed at the departmental level, which necessarily combines highly heterogeneous production systems. As a result, a given level of EDD may have different physiological and economic implications across cereal-dominated regions, viticultural areas, or livestock-based systems, as well as between lowland and mountainous environments. Beyond this productive heterogeneity, the EDD indicator itself captures exposure to absolute temperature levels rather than temperature anomalies relative to local climate conditions. The use of a common temperature threshold across space and time further reinforces this interpretation and, at our level of analysis, the threshold should be understood as a shared reference point for identifying episodes of extreme heat, not as a universal physiological damage threshold across crops, phenological stages, or climatic zones. Consequently, the estimated coefficients reflect average economic responses associated with local production mixes and exposure levels, rather than crop- or stage-specific biophysical mechanisms. Disentangling these underlying mechanisms lies beyond the scope of this analysis. In this respect, alternative definitions based on relative thresholds or local temperature percentiles commonly used in meteorological definitions of heatwaves offer a complementary way to characterize anomalous heat relative to local climate conditions, but they address a different economic question (Hsiang, 2016; Carleton et al., 2024). The spatial patterns identified in our analysis, particularly the more pronounced negative effects in inland areas characterized by livestock specialization and significant topographical constraints, are consistent with agronomic evidence emphasizing the structural vulnerability of these regions to climate-related stress (van der Velde et al., 2012).

Overall, this paper provides evidence that extreme heat has persistent and spatially heterogeneous effects on agricultural labor productivity in France. By combining high-resolution climate data with sector-specific exposure measures and a flexible econometric framework, we highlight regions where vulnerability to heat extremes appears particularly pronounced. Future research could build on this framework by incorporating additional agro-climatic indicators, exploiting finer spatial or sectoral data, or explicitly modeling adaptation and mitigation mechanisms (Burke and Emerick, 2016; Mérel and Gammans, 2021). Such extensions would further improve our understanding of how climate change affects agricultural productivity and how policy can support adaptation in the most exposed regions.

References

Ben-Ari, T., Boé, J., Ciais, P., Lecerf, R., van der Velde, M., and Makowski, D. (2018). Causes and implications of the unforeseen 2016 extreme yield loss in France's breadbasket. *Nature Communications*, 9:1627.

Berg, K. A., Curtis, C. C., and Mark, N. C. (2024). GDP and temperature: Evidence on cross-country response heterogeneity. *European Economic Review*, 169:104833.

Bolton, D. (1980). The computation of equivalent potential temperature. *Monthly Weather Review*, 108(7):1046–1053.

Bonnieux, F. (1982). Les disparités départementales de l'agriculture française de 1962 à 1980. *Économie rurale*, 152:34–39.

Bonnieux, F. and Rainelli, P. (1980). Les disparités départementales de l'agriculture française : essai d'explication. *Économie rurale*, 137:10–19.

Burke, M. and Emerick, K. (2016). Adaptation to climate change: Evidence from US agriculture. *American Economic Journal: Economic Policy*, 8(3):106–140.

Burke, M., Hsiang, S. M., and Miguel, E. (2015). Global non-linear effect of temperature on economic production. *Nature*, 527(7577):235–239.

Burke, M. and Tanutama, V. (2019). Climatic constraints on aggregate economic output. *NBER Working Paper*.

Butler, E. E., Mueller, N. D., and Huybers, P. (2018). Peculiarly pleasant weather for US maize. *Proceedings of the National Academy of Sciences*, 115(47):11935–11940.

Carleton, T., Duflo, E., Jack, B. K., and Zappalà, G. (2024). Adaptation to climate change. *Handbook of the Economics of Climate Change*, 1:143–248.

Ceglar, A., Toreti, A., Lecerf, R., van der Velde, M., and Dentener, F. (2016). Impact of meteorological drivers on regional inter-annual crop yield variability in France. *Agricultural and Forest Meteorology*, 216:58–67.

D'Agostino, A. L. and Schlenker, W. (2016). Recent weather fluctuations and agricultural yields: Implications for climate change. *Agricultural Economics*, 47(S1):159–171.

Damania, R., Desbureaux, S., and Zaveri, E. (2020). Does rainfall matter for economic growth? Evidence from global sub-national data (1990–2014). *Journal of Environmental Economics and Management*, 102:102335.

Dell, M., Jones, B. F., and Olken, B. A. (2012). Temperature shocks and economic growth: Evidence from the last half century. *American Economic Journal: Macroeconomics*, 4(3):66–95.

Dell, M., Jones, B. F., and Olken, B. A. (2014). What do we learn from the weather? The new climate-economy literature. *Journal of Economic Literature*, 52(3):740–798.

Deschênes, O. and Greenstone, M. (2007). The economic impacts of climate change: Evidence from agricultural output and random fluctuations in weather. *American Economic Review*, 97(1):354–385.

Devot, A., Royer, L., Arvis, B., Deryng, D., Caron Giauffret, E., Giraud, L., Ayral, V., and Rouillard, J. (2023). Research for AGRI Committee – The impact of extreme climate events on agricultural production in the EU. Technical Report IPOL_STU(2023)733115, European Parliament, Policy Department for Structural and Cohesion Policies, Brussels.

Gammans, M., Mérel, P., and Ortiz-Bobea, A. (2017). Negative impacts of climate change on cereal yields: statistical evidence from France. *Environmental Research Letters*, 12(5):054007.

Hatfield, J. L., Boote, K. J., Kimball, B. A., Ziska, L., Izaurralde, R. C., Ort, D., Thomson, A. M., and Wolfe, D. (2011). Climate impacts on agriculture: implications for crop production. *Agronomy Journal*, 103(2):351–370.

Haut Conseil pour le Climat (2024). Accélérer la transition climatique avec un système alimentaire bas carbone, résilient et juste. Technical report, Haut Conseil pour le Climat, Paris.

Hsiang, S. (2016). Climate econometrics. *Annual Review of Resource Economics*, 8:43–75.

IPCC (2021). *Climate Change 2021: The Physical Science Basis. Contribution of Working Group I to the Sixth Assessment Report of the Intergovernmental Panel on Climate Change*. Cambridge University Press, Cambridge, UK and New York, NY, USA.

IPCC (2022). *Climate Change 2022: Impacts, Adaptation and Vulnerability. Contribution of Working Group II to the Sixth Assessment Report of the Intergovernmental Panel on Climate Change*. Cambridge University Press, Cambridge, UK and New York, NY, USA.

Jordà, Ò. (2005). Estimation and inference of impulse responses by local projections. *American Economic Review*, 95(1):161–182.

Kahn, M. E., Mohaddes, K., Ng, R. N., Pesaran, M. H., Raissi, M., and Yang, J.-C. (2021). Long-term macroeconomic effects of climate change: A cross-country analysis. *Energy Economics*, 104:105624.

Kjellstrom, T., Briggs, D., Freyberg, C., Lemke, B., Otto, M., and Hyatt, O. (2016). Heat, human performance, and occupational health: A key issue for the assessment of global climate change impacts. *Annual Review of Public Health*, 37(1):97–112.

Lobell, D. B. and Asseng, S. (2017). Comparing estimates of climate change impacts from process-based and statistical crop models. *Environmental Research Letters*, 12(1):015001.

Lobell, D. B., Bänziger, M., Magorokosho, C., and Vivek, B. (2011). Nonlinear heat effects on African maize as evidenced by historical yield trials. *Nature Climate Change*, 1(1):42–45.

Mérel, P. and Gammans, M. (2021). Climate econometrics: Can the panel approach account for long-run adaptation? *American Journal of Agricultural Economics*, 103(4):1207–1238.

Midler, E. and Pagnon, J. (2022). Environment and climate assessment of france's cap strategic plan. Policy report, Institute for European Environmental Policy (IEEP), Brussels. Environment and climate assessment of France's CAP Strategic Plan.

Ministère de la Transition écologique et de la Cohésion des territoires (2025). Plan national d'adaptation au changement climatique 3 (PNACC-3) : préparer la France à +4 °C. Technical report, République française, Paris.

Muñoz Sabater, J. et al. (2019). ERA5-Land hourly data from 1981 to present. *Copernicus Climate Change Service (C3S) Climate Data Store (CDS)*, 10(10.24381).

Nóia Júnior, R. d. S., Deswarte, J.-C., Cohan, J.-P., Martre, P., van der Velde, M., Lecerf, R., Webber, H., Ewert, F., Ruane, A. C., Slafer, G. A., and Asseng, S. (2023). The extreme 2016 wheat yield failure in France. *Global Change Biology*, 29(11):3130–3146.

Olper, A., Maugeri, M., Manara, V., and Raimondi, V. (2021). Weather, climate and economic outcomes: Evidence from Italy. *Ecological Economics*, 189:107156.

Parent, B. and Tardieu, F. (2012). Temperature responses of developmental processes have not been affected by breeding in different ecological areas for 17 crop species. *New Phytologist*, 194(3):760–774.

Ribes, A., Boé, J., Qasmi, S., Dubuisson, B., Douville, H., and Terray, L. (2022). An updated assessment of past and future warming over France based on a regional observational constraint. *Earth System Dynamics*, 13(4):1397–1415.

Rosenzweig, C., Elliott, J., Deryng, D., Ruane, A. C., Müller, C., Arneth, A., Boote, K. J., Folberth, C., Glotter, M., Khabarov, N., et al. (2014). Assessing agricultural risks of climate change in the 21st century in a global gridded crop model intercomparison. *Proceedings of the national academy of sciences*, 111(9):3268–3273.

Rötter, R. and Van de Geijn, S. (1999). Climate change effects on plant growth, crop yield and livestock. *Climatic Change*, 43(4):651–681.

Schauberger, B., Makowski, D., Ben-Ari, T., Boé, J., and Ciais, P. (2021). No historical evidence for increased vulnerability of French crop production to climatic hazards. *Agricultural and Forest Meteorology*, 306:108453.

Schlenker, W. and Roberts, M. J. (2009). Nonlinear temperature effects indicate severe damages to US crop yields under climate change. *Proceedings of the National Academy of sciences*, 106(37):15594–15598.

Stull, R. (2011). Wet-bulb temperature from relative humidity and air temperature. *Journal of Applied Meteorology and Climatology*, 50(11):2267–2269.

Tack, J., Barkley, A., and Nalley, L. L. (2015). Effect of warming temperatures on US wheat yields. *Proceedings of the National Academy of Sciences*, 112(22):6931–6936.

van der Velde, M., Tubiello, F. N., Vrieling, A., and Bouraoui, F. (2012). Impacts of extreme weather on wheat and maize in France: evaluating regional crop simulations against observed data. *Climatic Change*, 113(3–4):751–765.

WMO (2024). State of the global climate 2023. *WMO: World Meteorological Organization.*

WMO (2025). State of the global climate 2024. *WMO: World Meteorological Organization.*

Zampieri, M., Ceglar, A., Dentener, F., and Toreti, A. (2017). Wheat yield loss attributable to heat waves, drought and water excess at the global, national and subnational scales. *Environmental Research Letters*, 12(6):064008.

A Online Appendix

A.1 Tables

Table A1: NUTS codes and names of all regions and departments in our database

NUTS	Name	NUTS	Name	NUTS	Name
FR1	Ile de France	FRF	Grand Est	FRJ12	Gard
FR101	Paris	FRF11	Bas-Rhin	FRJ13	Hérault
FR102	Seine-et-Marne	FRF12	Haut-Rhin	FRJ14	Lozère
FR103	Yvelines	FRF21	Ardennes	FRJ15	Pyrénées-Orientales
FR104	Essonne	FRF22	Aube	FRJ21	Ariège
FR105	Hauts-de-Seine	FRF23	Marne	FRJ22	Aveyron
FR106	Seine-Saint-Denis	FRF24	Haute-Marne	FRJ23	Haute-Garonne
FR107	Val-de-Marne	FRF31	Meurthe-et-Moselle	FRJ24	Gers
FR108	Val-d'Oise	FRF32	Meuse	FRJ25	Lot
FRB	Centre-Val de Loire	FRF33	Moselle	FRJ26	Hautes-Pyrénées
FRB01	Cher	FRF34	Vosges	FRJ27	Tarn
FRB02	Eure-et-Loir	FRG	Pays de la Loire	FRJ28	Tarn-et-Garonne
FRB03	Indre	FRG01	Loire-Atlantique	FRK	Auvergne-Rhône-Alpes
FRB04	Indre-et-Loire	FRG02	Maine-et-Loire	FRK11	Allier
FRB05	Loir-et-Cher	FRG03	Mayenne	FRK12	Cantal
FRB06	Loiret	FRG04	Sarthe	FRK13	Haute-Loire
FRC	Bourgogne-Franche-Comté	FRG05	Vendée	FRK14	Puy-de-Dôme
FRC11	Côte-d'Or	FRH	Bretagne	FRK21	Ain
FRC12	Nièvre	FRH01	Côtes-d'Armor	FRK22	Ardèche
FRC13	Saône-et-Loire	FRH02	Finistère	FRK23	Drôme
FRC14	Yonne	FRH03	Ille-et-Vilaine	FRK24	Isère
FRC21	Doubs	FRH04	Morbihan	FRK25	Loire
FRC22	Jura	FRI	Nouvelle-Aquitaine	FRK26	Rhône
FRC23	Haute-Saône	FRI11	Dordogne	FRK27	Savoie
FRC24	Territoire de Belfort	FRI12	Gironde	FRK28	Haute-Savoie
FRD	Normandie	FRI13	Landes	FRL	Provence-Alpes-Côte d'Azur
FRD11	Calvados	FRI14	Lot-et-Garonne	FRL01	Alpes-de-Haute-Provence
FRD12	Manche	FRI15	Pyrénées-Atlantiques	FRL02	Hautes-Alpes
FRD13	Orne	FRI21	Corrèze	FRL03	Alpes-Maritimes
FRD21	Eure	FRI22	Creuse	FRL04	Bouches-du-Rhône
FRD22	Seine-Maritime	FRI23	Haute-Vienne	FRL05	Var
FRE	Hauts-de-France	FRI31	Charente	FRL06	Vaucluse
FRE11	Nord	FRI32	Charente-Maritime	FRM	Corse
FRE12	Pas-de-Calais	FRI33	Deux-Sèvres	FRM01	Corse-du-Sud
FRE21	Aisne	FRI34	Vienne	FRM02	Haute-Corse
FRE22	Oise	FRJ	Occitanie		
FRE23	Somme	FRJ11	Aude		

Note: The NUTS nomenclature is organized into three levels (NUTS1 regional, NUTS2 intermediate, NUTS3 departmental). For France, the regional and departmental levels are the most relevant. They are represented by a NUTS code with 3 (region) or 5 (department) characters. For our analysis we focus only on departments. We exclude four departments (FR101, FR105, FR106, and FR107) due to negligible agricultural production (zero or near-zero). The final sample comprises 92 departments ($N = 92$).

Table A2: Distributions of $\beta_{r,h}$ (baseline and control specifications), p-values

Specification	h	KS test	MWU test	h	KS test	MWU test
1	0	0.955	0.469	3	0.004 **	0.016 *
	1	0.880	0.316	4	0.059	0.056
	2	0.238	0.175	5	0.416	0.301
2	0	0.319	0.154	3	0.001 **	0.001 ***
	1	0.059	0.033 *	4	0.039 *	0.062
	2	0.319	0.083	5	0.174	0.064
3	0	0.238	0.183	3	0.652	0.964
	1	0.059	0.151	4	0.774	0.437
	2	0.319	0.331	5	0.880	0.613
4	0	0.955	0.992	3	0.000 ***	0.003 **
	1	0.774	0.466	4	0.416	0.436
	2	0.416	0.410	5	0.880	0.598
5	0	0.774	0.724	3	0.238	0.405
	1	0.652	0.911	4	0.174	0.140
	2	0.319	0.145	5	0.086	0.070
6	0	0.652	0.353	3	0.004 **	0.012 *
	1	0.086	0.064	4	0.002 **	0.002 **
	2	0.086	0.024 *	5	0.124	0.054
7	0	0.652	0.491	3	0.652	0.992
	1	0.174	0.415	4	0.238	0.106
	2	0.955	0.695	5	0.774	0.429
8	0	0.529	0.390	3	0.416	0.600
	1	0.319	0.372	4	0.990	0.887
	2	0.955	0.955	5	0.955	0.770
9	0	0.774	0.992	3	0.319	0.714
	1	0.529	0.878	4	0.039 *	0.010 *
	2	0.238	0.065	5	0.124	0.041 *

Note: Numbers in the 'Specification' column correspond to the following control specifications: 1 = admin, 2 = influence, 3 = rain, 4 = marketVA, 5 = influence + rain, 6 = influence + admin, 7 = rain + admin, 8 = marketVA + rain, 9 = influence + rain + admin. This table shows, for each horizon h, the p-values from the Kolmogorov-Smirnov test (KS) test and the Mann-Whitney U test (MWU) test comparing the $\beta^{\iota}_{r,h}$ coefficients between the baseline and each control specification. For the KS test the null hypothesis is that the samples are drawn from the same distribution. For the MWU test, the null hypothesis is that the distributions of both samples are identical. Significance levels are indicated as follows: *** $p < 0.001$, ** $p < 0.01$, * $p < 0.05$. *Sources*: ERA5-Land, ARDECO, CORINE Land Cover, and Eurostat

Table A3: Distributions of significant $\beta_{r,h}$ only (baseline and control specifications), p-values

Specification	h	KS test	MWU test	h	KS test	MWU test
1	0	0.508	0.160	3	0.725	0.731
	1	0.431	0.129	4	0.155	0.327
	2	0.932	0.975	5	0.504	0.243
2	0	0.393	0.218	3	0.139	0.307
	1	0.358	0.274	4	0.500	0.984
	2	0.486	0.240	5	0.281	0.235
3	0	0.937	0.888	3	0.191	0.057
	1	0.659	0.795	4	0.438	0.149
	2	0.980	0.882	5	0.666	0.660
4	0	0.216	0.039 *	3	0.628	0.888
	1	0.279	0.124	4	0.564	0.940
	2	0.101	0.089	5	0.051	0.020 *
5	0	1.000	0.886	3	0.490	0.262
	1	0.774	0.954	4	0.361	0.786
	2	0.817	0.666	5	0.518	0.872
6	0	0.371	0.150	3	0.595	0.492
	1	0.957	0.698	4	0.353	0.429
	2	0.244	0.248	5	0.256	0.077
7	0	0.956	0.722	3	0.315	0.220
	1	0.292	0.484	4	0.944	0.923
	2	0.953	0.928	5	0.916	0.839
8	0	0.871	0.376	3	0.442	0.376
	1	0.946	0.881	4	0.763	0.648
	2	0.769	0.310	5	0.581	0.332
9	0	0.750	0.815	3	0.181	0.058
	1	0.420	0.817	4	0.823	0.757
	2	0.756	0.822	5	0.475	0.505

Note: Numbers in the 'Specification' column correspond to the following control specifications: 1 = admin, 2 = influence, 3 = rain, 4 = marketVA, 5 = influence + rain, 6 = influence + admin, 7 = rain + admin, 8 = marketVA + rain, 9 = influence + rain + admin. This table shows, for each horizon h, the p-values from the Kolmogorov-Smirnov test (KS) test and the Mann-Whitney U test (MWU) test comparing the $\beta^{\Gamma}_{r,h}$ coefficients between the baseline and each control specification. For the KS test the null hypothesis is that the samples are drawn from the same distribution. For the MWU test, the null hypothesis is that the distributions of both samples are identical. Significance levels are indicated as follows: *** $p < 0.001$, ** $p < 0.01$, * $p < 0.05$. *Sources*: ERA5-Land, ARDECO, CORINE Land Cover, and Eurostat

A.2 Figures

Figure A1: NUTS3 delimitations for France and temperature for January 1, 2000 at 12 AM

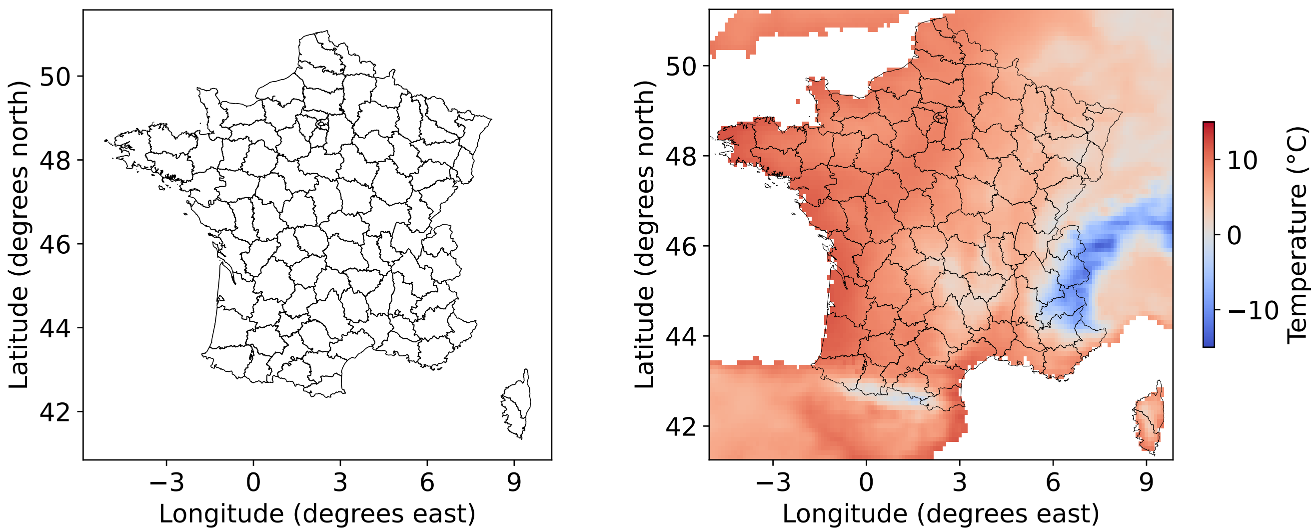

(a) NUTS3 (b) Data obtained

Note: (a) For France, NUTS3 boundaries correspond to the administrative departments of the country. (b) Example of the resulting dataset. Each grid cell represents 0.1° x 0.1° (≈ 9 x 9 km). The boundaries correspond to departments (NUTS3). *Source*: ERA5-Land.

Figure A2: CORINE Land Cover nomenclature

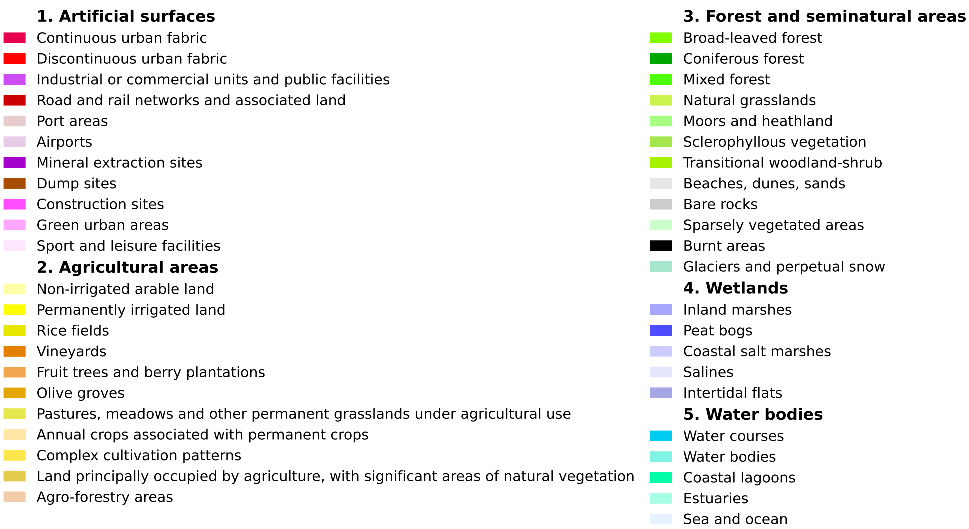

Note: Nomenclature of the CORINE Land Cover dataset. *Source*: CORINE Land Cover.

Figure A3: Annual sector-specific EDD for France and its departments, 1980-2023

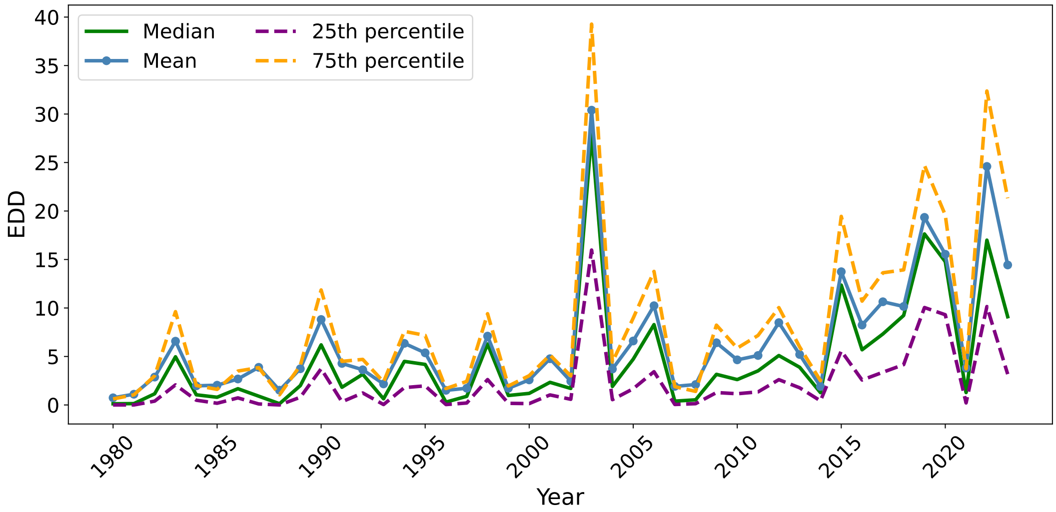

Note: Annual sector-specific EDD for France and its departments over the period 1980–2023. The series is based on high-resolution ERA5-Land reanalysis data, combined with CORINE Land Cover to isolate agricultural areas. The chart shows the median (green), mean (blue), 25th percentile (purple), and 75th percentile (orange) of the departmental EDD distribution for each year. *Sources*: ERA5-Land and CORINE Land Cover.

Figure A4: Daily sector-specific EDD evolution for France, 1980-2023

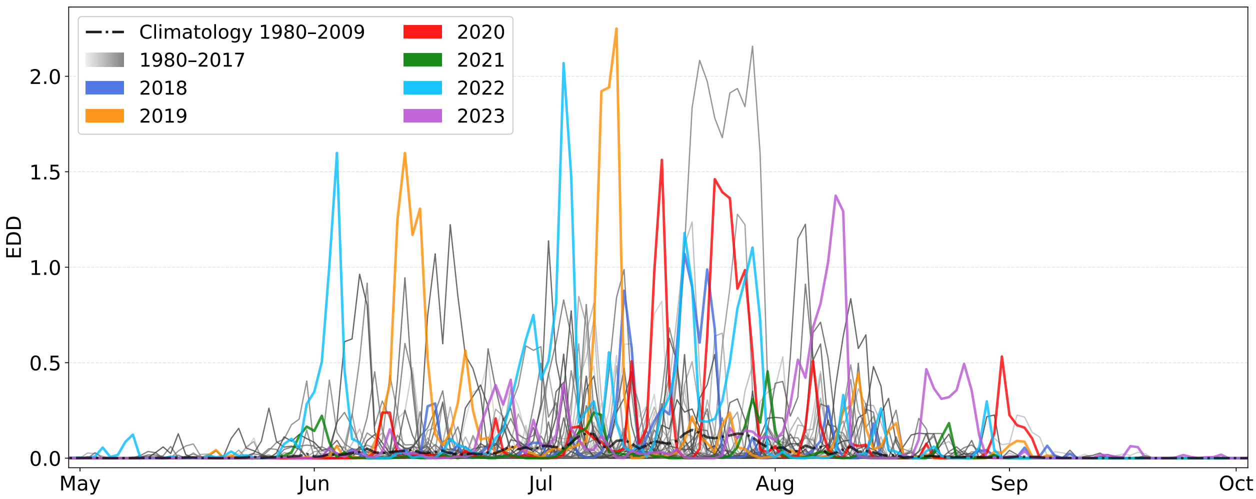

Note: Daily sector-specific EDD evolution for France over the period 1980-2023 and averaged nationally. The series is based on high-resolution ERA5-Land reanalysis data, combined with CORINE Land Cover to isolate agricultural areas. The chart shows, for each month, the daily evolution for the 1980-2017 period (gray gradient), the last six years (diverse colors), and the climatological mean for 1980–2009 (black dashed line). Days outside these months have no EDD. *Sources*: ERA5-Land and CORINE Land Cover.

Figure A5: Main and secondary technical and economic organization of farms (OTEX) in 2010

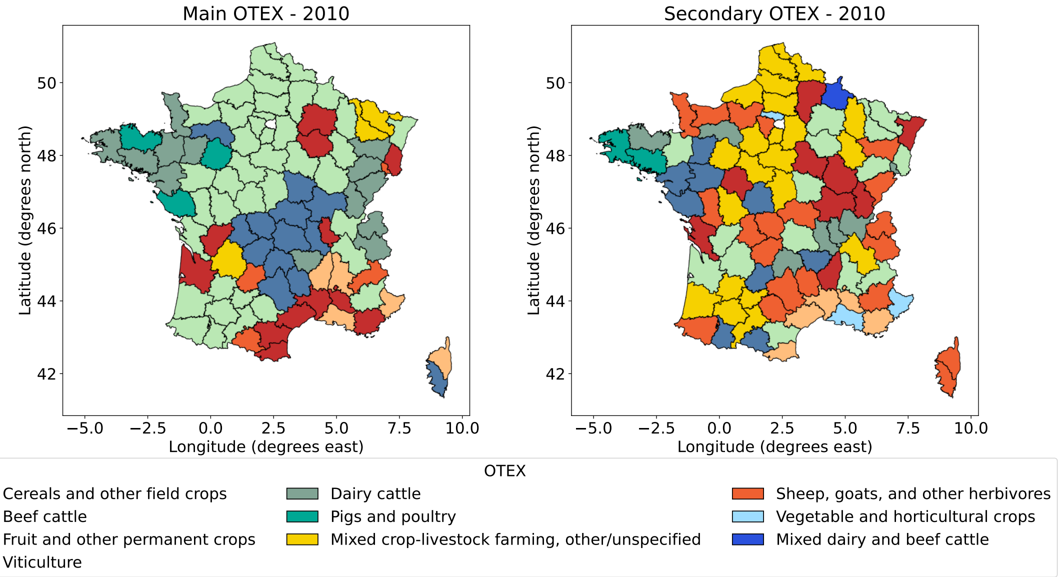

Note: We calculate the share of each category of technical and economic organization of farms for each department based on the number of farms in each category. For 2010 the main (left) and secondary (right) OTEX is highlighted. *Sources*: Agricultural Census 2010.

Figure A6: Main and secondary technical and economic organization of farms (OTEX) in 2020

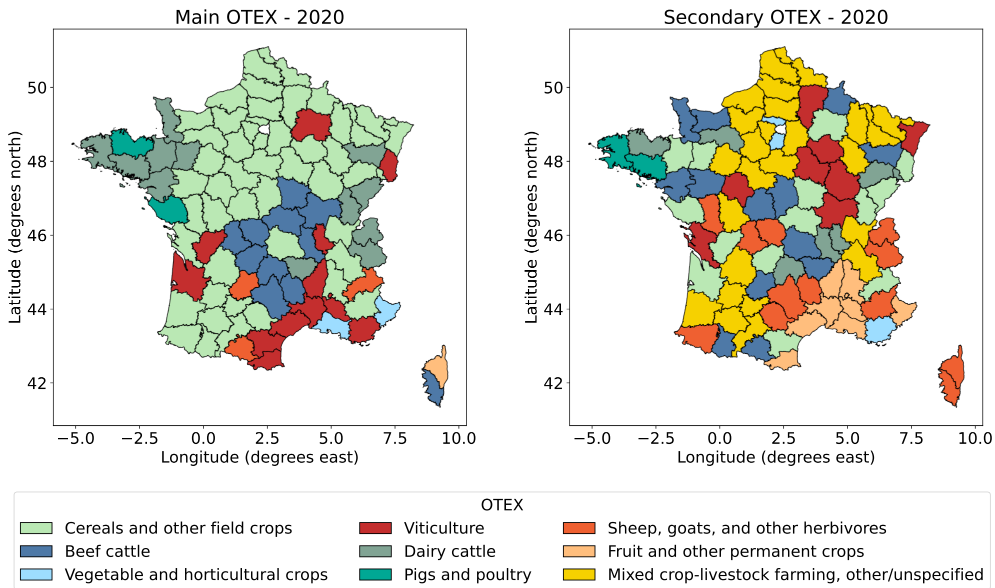

Note: We calculate the share of each category of technical and economic organization of farms for each department based on the number of farms in each category. For 2020 the main (left) and secondary (right) OTEX is highlighted. *Sources*: Agricultural Census 2020.

Figure A7: Detailed impulse-responses for $\beta_{r,h}$ by department (1/3)

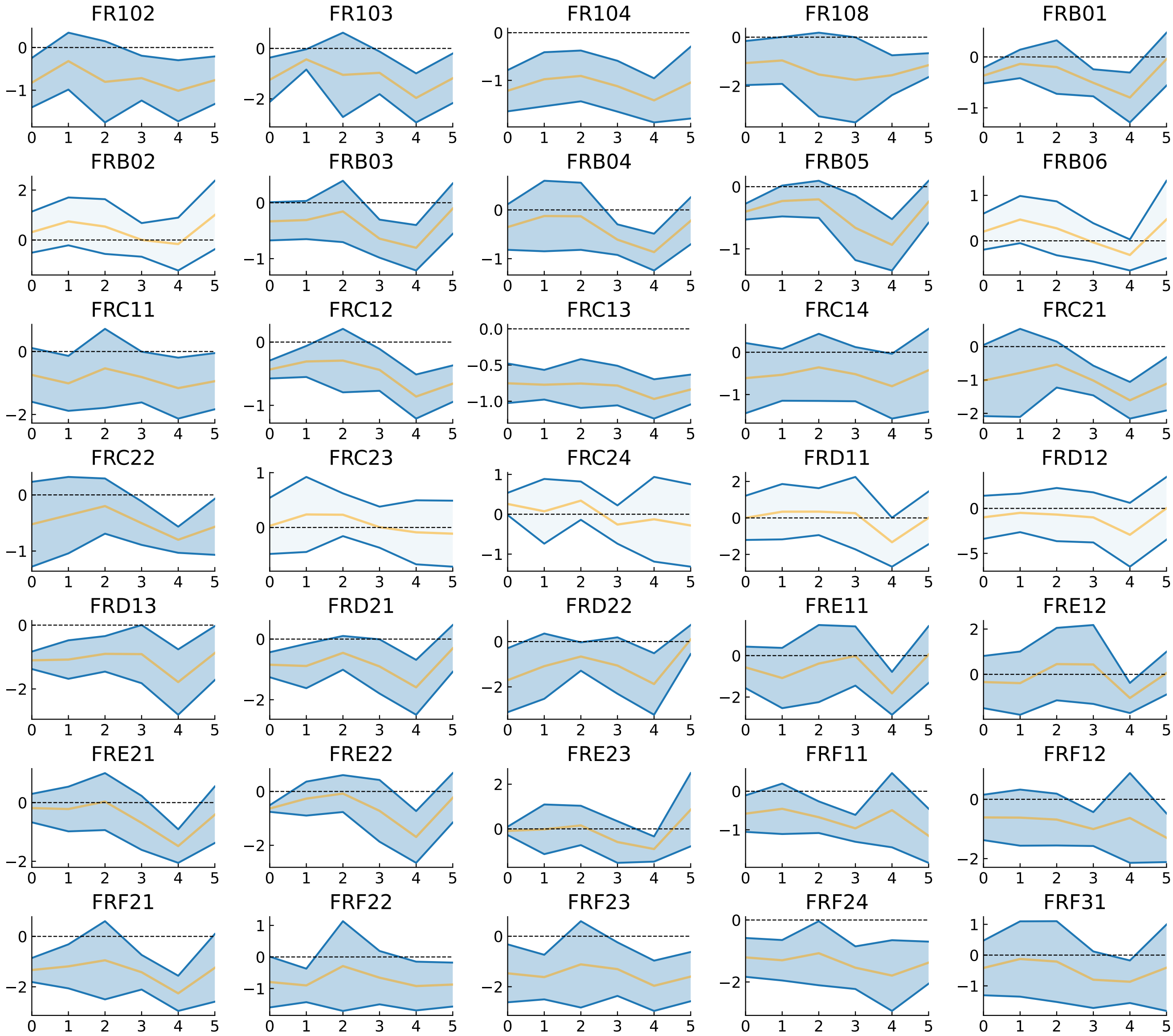

Note: Each subplot represents, for one department, the evolution of the sector-specific EDD coefficient, $\beta_{r,h}$, estimated from Equation 4. The yellow line shows the point estimate, and the blue lines denote the 95% confidence interval. When at least a horizon is significant at the 5% level (i.e., the 95% interval excludes zero), the area between the estimate and the interval is shaded in darker blue. The NUTS code for the department is displayed above each subplot. *Sources*: ERA5-Land and ARDECO.

Figure A7: Detailed impulse-responses for $\beta_{r,h}$ by department (2/3)

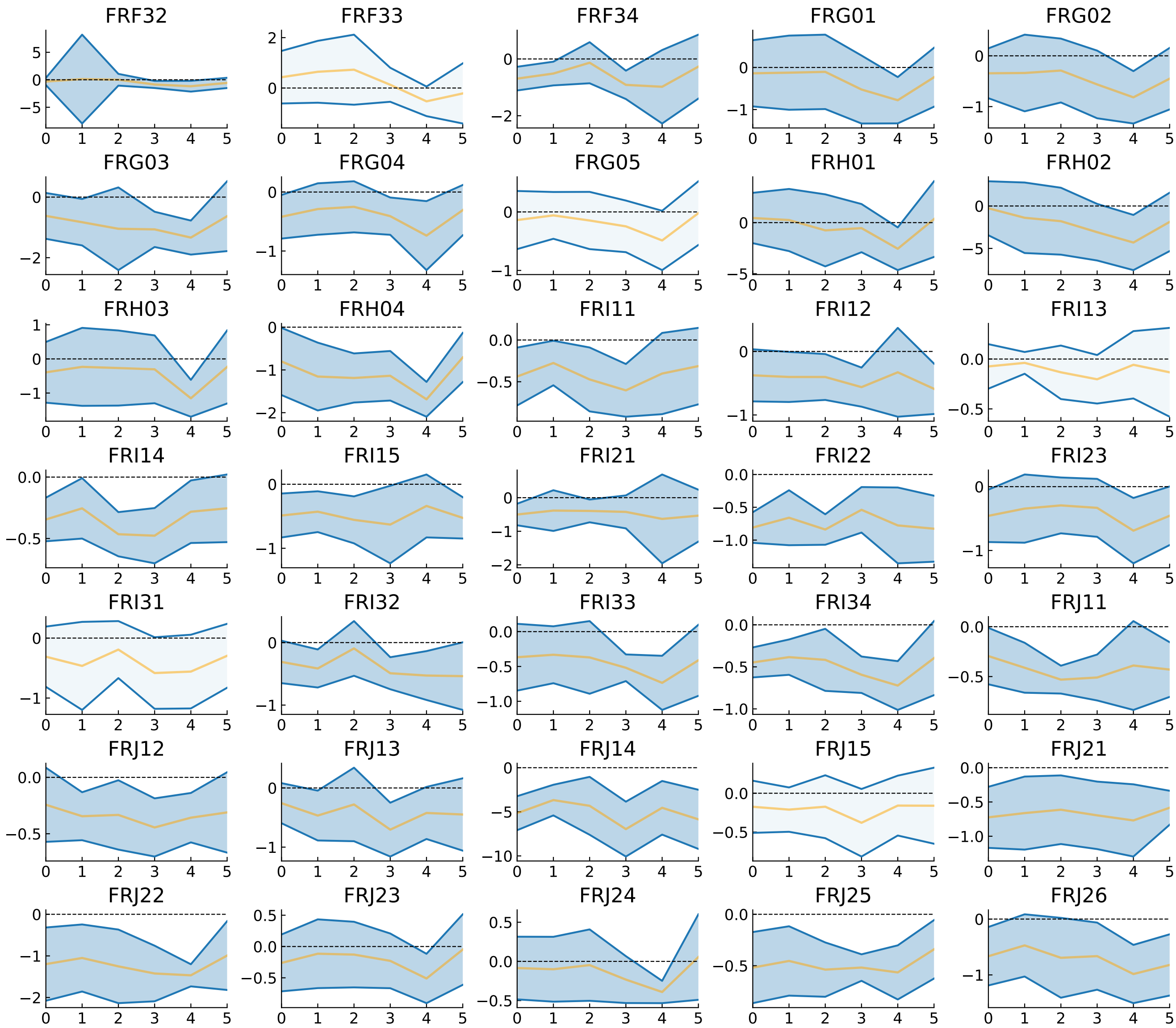

Note: Each subplot represents, for one department, the evolution of the sector-specific EDD coefficient, $\beta_{r,h}$, estimated from Equation 4. The yellow line shows the point estimate, and the blue lines denote the 95% confidence interval. When at least a horizon is significant at the 5% level (i.e., the 95% interval excludes zero), the area between the estimate and the interval is shaded in darker blue. The NUTS code for the department is displayed above each subplot. *Sources*: ERA5-Land and ARDECO.

Figure A7: Detailed impulse-responses for $\beta_{r,h}$ by department (3/3)

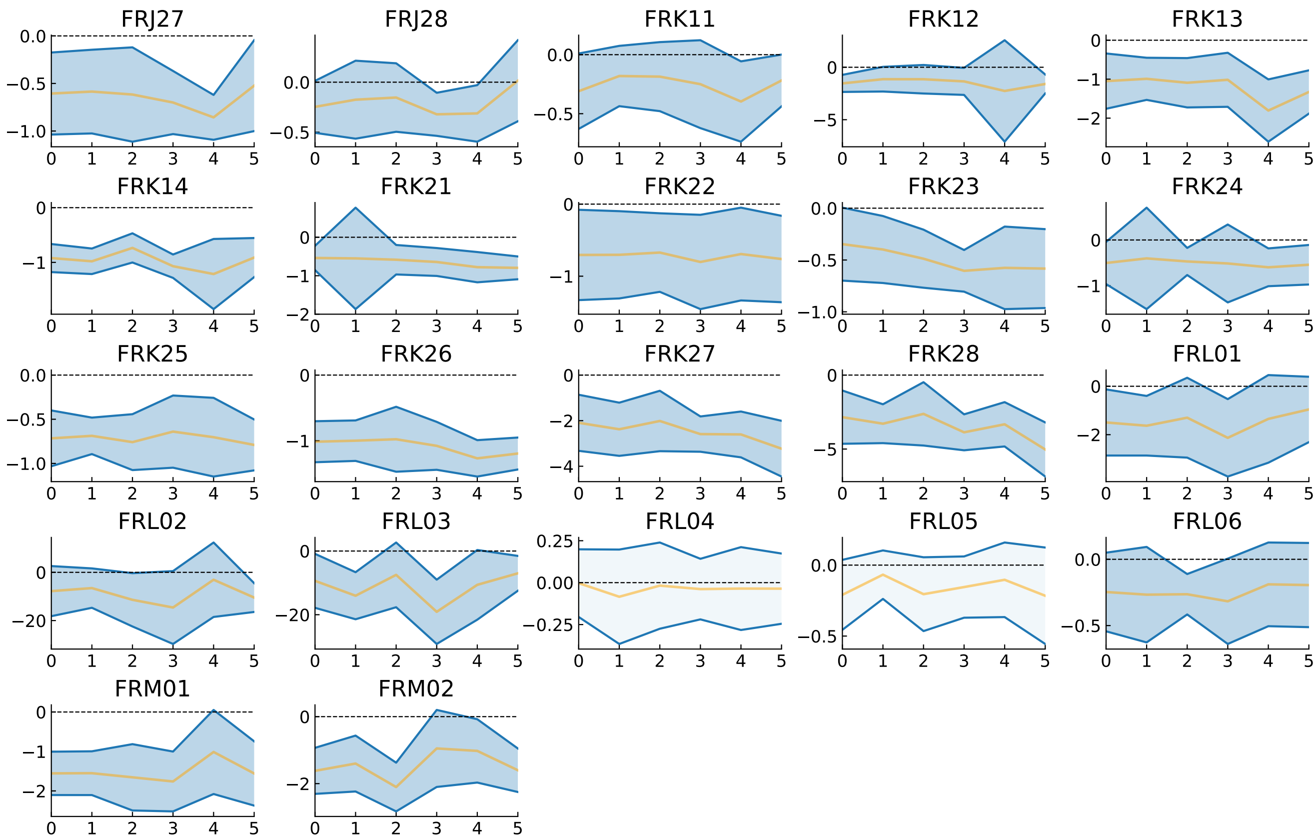

Note: Each subplot represents, for one department, the evolution of the sector-specific EDD coefficient, $\beta_{r,h}$, estimated from Equation 4. The yellow line shows the point estimate, and the blue lines denote the 95% confidence interval. When at least a horizon is significant at the 5% level (i.e., the 95% interval excludes zero), the area between the estimate and the interval is shaded in darker blue. The NUTS code for the department is displayed above each subplot. *Sources*: ERA5-Land and ARDECO.

A.3 Humidity-adjusted Extreme Degree Days

A.3.1 Construction of the wet-bulb indicator

To account for atmospheric humidity in the measurement of extreme heat exposure, we construct an alternative indicator based on wet-bulb temperature. Wet-bulb temperature T^{wb} combines air temperature and humidity and better reflects thermal stress under humid conditions.

Using hourly ERA5-Land data on 2-meter air temperature T and 2-meter dew point temperature T^d, we first compute relative humidity. Saturation vapor pressure is computed using the approximation of Bolton (1980):

$$e_s(T) = 6.112 \exp\left(\frac{17.67T}{T + 243.5}\right). \tag{10}$$

Relative humidity is derived from its thermodynamic definition as:

$$RH = 100 \times \frac{e_s(T^d)}{e_s(T)}, \tag{11}$$

where T^d denotes dew point temperature.

Wet-bulb temperature is then approximated using the closed-form expression proposed by Stull (2011):

$$\begin{aligned} T^{wb} \approx\ & T \arctan\left(0.151977\sqrt{RH + 8.313659}\right) \\ & + \arctan(T + RH) - \arctan(RH - 1.676331) \\ & + 0.00391838\, RH^{3/2} \arctan(0.023101\, RH) - 4.686035. \end{aligned} \tag{12}$$

A.3.2 Definition of humidity-adjusted EDD

We define humidity-adjusted EDD analogously to the baseline dry-bulb specification. Let τ denote a wet-bulb temperature threshold. The hourly excess temperature is:

$$EDD_t^{wb} = \max\left(T_t^{wb} - \tau, 0\right), \tag{13}$$

which is aggregated to daily and then monthly values, and finally summed at the annual level.

To ensure strict comparability with the baseline 29 °C dry-bulb threshold, the wet-bulb threshold τ is calibrated such that:

$$\Pr(T > 29\ °\mathrm{C}) = \Pr(T^{wb} > \tau), \tag{14}$$

computed over all hours and grid cells in France during the period 1980-2023. This frequency-equivalence approach guarantees that both measures capture extreme heat events of comparable national rarity. Monthly wet-bulb EDD values are spatially aggregated at the departmental level using the same agricultural land-use weights as in the baseline specification.

A.3.3 Estimation results

We report the comparison of baseline and humidity-adjusted EDD distributions by horizon in Figure A8, and their geographical distribution in Figure A9. Re-estimating the local projections using the humidity-adjusted indicator yields impulse responses that remain qualitatively close to the baseline results. The dynamic profile of negative effects persists, and the spatial concentration of impacts in inland and livestock-oriented regions is largely preserved.

Although point estimates are generally larger in magnitude, statistical significance is reduced at some horizons. Two elements may contribute to these differences. First, the wet-bulb temperature is computed using a closed-form approximation, which may introduce additional measurement noise relative to the baseline specification. Second, the calibrated wet-bulb threshold ($\tau = 20.63$ °C) is mechanically lower than the 29 °C baseline, implying that a one-unit increase in the humidity-adjusted EDD corresponds to a relatively larger thermal anomaly. As a result, coefficient magnitudes are not directly comparable in scale across specifications.

Overall, the consistency of the dynamic responses and spatial patterns indicates that the baseline findings are not driven solely extreme temperature exposure and remain robust to accounting for atmospheric humidity.

Figure A8: Alternative measure of EDD (humidity-adjusted), comparison between $\beta_{r,h}$ and $\beta^{wb}_{r,h}$

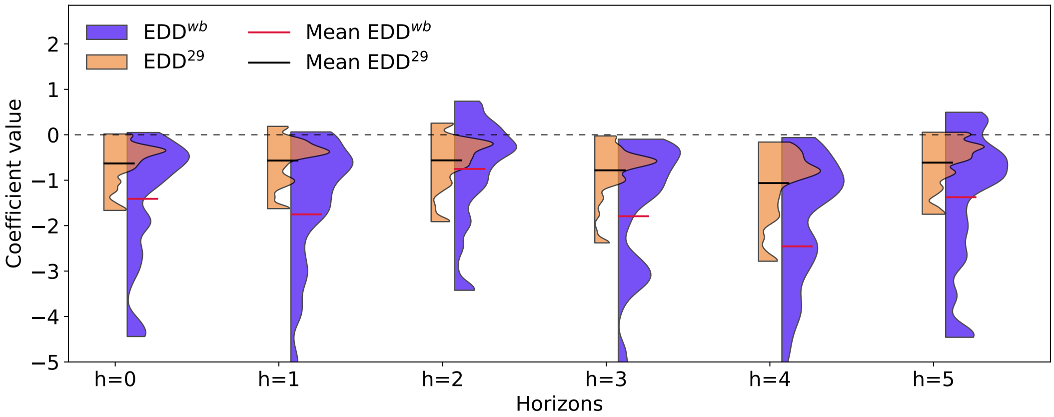

Note: For each horizon we present the distributions of estimate derived from equations (4) for different EDD measures (usual temperature and humidity-adjusted temperature). The distribution of baseline measure (29 °C) coefficients $\beta_{r,h}$ is shown in orange and distributions of alternative measure (humidity-adjusted or wet-bulb) coefficients $\beta^{wb}_{r,h}$ are in purple. The mean estimates are indicated with a black and red lines respectively in the associated distributions. Data are winsorized. Low values are truncated to improve visual. *Sources*: ERA5-Land, ARDECO, and CORINE Land Cover.

Figure A9: Estimated humidity-adjusted EDD impacts $\beta^{wb}_{r,h}$ by horizon

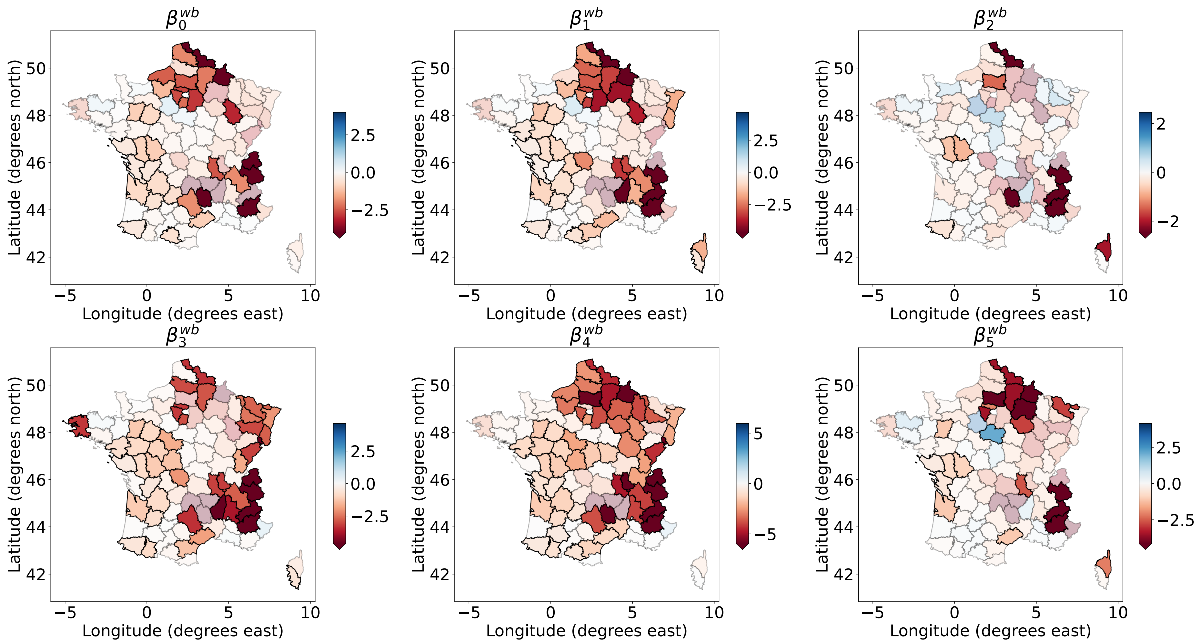

Note: Each panel shows the departmental-level coefficient $\beta^{wb}_{r,h}$ estimated from the robustness to humidity-adjusted heat exposure, corresponding to a forecast horizon $h \in \{0, \ldots, 5\}$. Shading intensity reflects the magnitude and direction of the estimated effect. Red hues indicate negative impacts and blue hues indicate positive impacts. Statistically significant coefficients are shown in opaque colors, while transparent areas indicate non-significance. Color scales vary by panel to accommodate differences in magnitude. Extreme values are truncated for legibility. *Sources*: ERA5-Land, ARDECO, and CORINE Land Cover.